OPTIMIZING RADIATION DOSE AND IMAGE QUALITY IN A MULTI-DETECTOR COMPUTED TOMOGRAPHY

PIMOLPUN CHANGKAEW

A THESIS SUBMITTED IN PARTIAL FULFILLMENT
OF THE REQUIREMENTS FOR
THE DEGREE OF MASTER OF SCIENCE (MEDICAL PHYSICS)
FACULTY OF GRADUATE STUDIES
MAHIDOL UNIVERSITY
2005

ISBN 974-04-6314-2

Thesis
Entitled

OPTIMIZING RADIATION DOSE AND IMAGE QUALITY IN A MULTI-DETECTOR COMPUTED TOMOGRAPHY

Pimolpun Changkaew
Miss Pimolpun Changkaew
Candidate

Dr. Napapong Pongnapang,
Ph.D.(Medical Physics)
Major-Advisor

Assoc.Prof. Manus Mongkolsuk,
M.Sc.(Physics)
Co-Advisor

Miss Sawwanee Asavaphatiboon,
M.Sc.(Medical Physics)
Co-Advisor

Miss Nuttawan Jang-sri,
M.Sc.(Radiological Science)
Co-Advisor

Assoc.Prof. Rassmidara Hoonsawat,
Ph.D.
Dean
Faculty of Graduate Studies

Assoc.Prof. Vipa Boonkitticharoen,
Ph.D.(Radiation Radiology)
Chair
Master of Science Programme
in Medical Physics
Faculty of Medicine,
Ramathibodi Hospital

Thesis
Entitled

OPTIMIZING RADIATION DOSE AND IMAGE QUALITY IN A MULTI-DETECTOR COMPUTED TOMOGRAPHY

was submitted to the Faculty of Graduate Studies, Mahidol University
For the degree of Master of Science (Medical Physics)
on
June 3, 2005

Pimolpun Changkaew
Miss Pimolpun Changkaew
Candidate

Dr. Napapong Pongnapang,
Ph.D.(Medical Physics)
Chair

Assoc.Prof. Chavalit Wongse-ek,
M.Sc.(Physics)
Member

Assoc.Prof. Manus Mongkolsuk,
M.Sc.(Physics)
Member

Miss Sawwanee Asavaphatiboon,
M.Sc.(Medical Physics)
Member

Miss Nuttawan Jang-sri,
M.Sc.(Radiological Science)
Member

Assoc.Prof. Rassmidara Hoonsawat,
Ph.D.
Dean
Faculty of Graduate Studies,
Mahidol University

Prof. Rajata Rajatanavin,
M.D., F.A.C.E.
Professor of Medicine,
Dean,
Faculty of Medicine
Ramathibodi Hospital,
Mahidol University.

ACKNOWLEDGEMENT

The success of this thesis can been attributed to the extensive support and assistance from my major advisor, Dr. Napapong Pongnapang and my co-advisor, Assoc. Prof. Manus Mongkolsuk (Department of Radiology, Faculty of Medical Technology, Mahidol University). I wish to thank them for their valuable advice, guidance, constructive comments, English language proof and helpful support using of the new arrival NOMEX electrometer and ionization chamber in this research study.

I would like to deeply thank Archan Sawwanee Asavaphatiboon (Department of Radiology, Sirikit Medical Center, Ramathibodi Hospital), Archan Nuttawan Jang-sri (Department of Radiology, Taksin Hospital) my co-advisor for their helpful support on using of the research instrument (MDCT and phantoms) and providing suggestions for improvement.

I would like to sincere the committee of this thesis, Assoc. Prof. Chavalit Wongse-ek (Department of Radiology, Faculty of Medical Technology, Mahidol University) for his kindness in examining this thesis and valuable suggestions for improvement.

I wish to thank Mr. Vichan Prasertsilapakul and all staffs of the AIMC center, Ramathibodi Hospital for their helpful support and kind co-operation in using MDCT during the entire experiment. I also wish to thank Mr. Samrit Kittipayak for his willing help me doing all through the experiment. And I wish to thank Miss Supranee Supanunt for her kindly support on digital camera.

I am grateful to all the teachers, lecturers and staffs in the School of Medical Physics at Division of Radiation Oncology and Nuclear Medicine, Ramathibodi Hospital for their kind support and supply the academic knowledge on medical physics.

Finally, I am grateful to my family and all friends for their love, care and support thought this course of study.

Pimolpun Changkaew

OPTIMIZING RADIATION DOSE AND IMAGE QUALITY IN A MULTI-DETECTOR COMPUTED TOMOGRAPHY

PIMOLPUN CHANGKAEW 4436396 RAMP/M

M.Sc. (MEDICAL PHYSICS)

THESIS ADVISORS: NAPAPONG PONGNAPANG, Ph.D. (MEDICAL PHYSICS), MANUS MONGKOLSUK, M.Sc. (PHYSICS), SAWWANEE ASAVAPHATIBOON, M.Sc. (MEDICAL PHYSICS), NUTTAWAN JANGSRI, M.Sc. (RADIOLOGICAL SCIENCE)

ABSTRACT

The study was carried out to find optimal scanning parameters for an MDCT at Ramathibodi hospital. A Phantom model was employed to assess image quality and standard ionization chamber was used to measure radiation dose. Tube current, slice thickness, pixel size and pitch were varied from routine techniques to evaluate factors affecting image quality (spatial resolution, contrast and noise) and dose (DLP_{air}) with aim of optimization.

Results from our study showed that, optimization of radiation dose and image quality could be achieved by proper selection of scanning parameters. Reduction of tube current could be made 22 - 28%, pitch could be doubled from 0.75 to 1.5 (50% dose reduction) in slice thickness less than 7.5 mm without any significant effects on noise and contrast. In examinations that do not require high spatial resolution, larger pixel size could be made and could result in 15 - 17% dose reduction.

We concluded from our study that, optimal scanning parameters were 115, 105, 150 and 170 mA for head (above/below posterior fossa) and abdomen (pre and post- contrast) protocols, respectively. Slice thickness should be made thinnest possible before the penumbra dose penalty becomes significant. Pitch and pixel size should be selected based on clinical requirements.

KEY WORDS: MULTI-DETECTOR CT / OPTIMIZATION / IMAGE QUALITY / RADIATION DOSE

87 P. ISBN 974-04-6314-2

การปรับค่าปริมาณรังสีให้เหมาะสมกับคุณภาพของภาพในเครื่องเอกซเรย์คอมพิวเตอร์ชนิดหลายหัววัด (OPTIMIZING RADIATION DOSE AND IMAGE QUALITY IN A MULTI-DETECTOR COMPUTED TOMOGRAPHY)

พิมลพรรณ ช้างแก้ว 4436396 RAMP/M

วท.ม. (ฟิสิกส์การแพทย์)

คณะกรรมการควบคุมวิทยานิพนธ์: นภาพงษ์ พงษ์นภางค์ Ph.D. (Medical Physics), มานัส มงคลสุข วท.ม. (ฟิสิกส์), เสาวนีย์ อัศวผาติบุญ, วท.ม. (ฟิสิกส์การแพทย์), ฉัฐวรรณ แจ้งสี, วท.ม. (วิทยาศาสตร์รังสี)

บทคัดย่อ

งานวิจัยนี้มุ่งศึกษาหาค่าพารามิเตอร์ในการสแกนที่เหมาะสมสำหรับเครื่องซีทีระบบหลายหัววัด ณ โรงพยาบาลรามาธิบดี ซึ่งในครั้งนี้ได้ทำการศึกษาถึงผลของการเปลี่ยนแปลงค่าพารามิเตอร์ในการสแกน ที่มีต่อคุณภาพของภาพและปริมาณรังสีในเครื่องซีทีระบบหลายหัววัดของโรงพยาบาลรามาธิบดี เพื่อนำไปสู่การปรับเปลี่ยนค่าพารามิเตอร์ต่างๆ ให้เหมาะสม หุ่นจำลองได้ถูกนำมาใช้ในการประเมินคุณภาพของภาพ และหัววัดรังสีได้ถูกนำมาใช้วัดปริมาณรังสี โดยปัจจัยที่มีผลต่อคุณภาพของภาพและปริมาณรังสีที่ทำการศึกษาในครั้งนี้ ได้แก่ กระแสหลอด ความหนาของสไลด์ ขนาดของพิกซัล และพิตช์ โดย ความคมชัด คอนทราส และ สัญญาณรบกวน เป็นตัวประเมินคุณภาพของภาพ ส่วน DLP_{air} เป็นค่าที่ได้จากการวัดปริมาณรังสี

จากการศึกษาพบว่าการปรับค่าปริมาณรังสีให้เหมาะสมกับคุณภาพของภาพสามารถทำได้โดยการปรับพารามิเตอร์ต่างๆ ดังกล่าวข้างต้นดังนี้ กระแสหลอดสามารถลดได้ 22 - 28% พิตช์สามารถเพิ่มจาก 0.75 เป็น 1.5 (ลดปริมาณรังสี 50%) ในความหนาของการตัดภาพที่น้อยกว่า 7.5 มม โดยไม่มีผลต่อระดับคอนทราสและสัญญาณรบกวน ในการตรวจที่ไม่ต้องการความคมชัดมากนัก สามารถเพิ่มขนาดพิกเซลได้ โดยสามารถลดปริมาณรังสีลง 15 - 17%

เราสรุปผลจากการศึกษาครั้งนี้ว่าค่าพารามิเตอร์ที่เหมาะสมในการสแกนได้แก่ 115, 105, 150 และ 170 มิลลิแอมแปร์ สำหรับการตรวจศีรษะเหนือและใต้ posterior fossa การตรวจช่องท้อง ก่อนและหลังการฉีดสารทึบรังสีตามลำดับ ความหนาของการตัดควรทำให้บางเท่าที่จะทำได้ก่อนที่จะทำให้ปริมาณรังสีเพิ่มขึ้นอย่างมีนัยสำคัญ พิตช์และขนาดพิกซัลควรเลือกให้เหมาะสมตามลักษณะการตรวจทางคลินิค

87 หน้า ISBN 974-04-6314-2

CONTENTS

LIST OF TABLES

LIST OF TABLES (Continued)

LIST OF FIGURES

LIST OF FIGURES (Continued)

LIST OF FIGURES (Continued)

LIST OF ABBREVIATIONS

Abbreviation	Term
ALARA	As low as reasonably achievable
cm	Centimeter
CTDI	Computed tomography dose index
$CTDI_{air}$	Computed tomography dose index free in air at the axis of the rotation
$CTDI_w$, $CTDI_{100w}$	Weighted computed tomography dose index
$CTDI_{100}$	CTDI, conveniently assessed using a pencil ionization chamber with an active length of 100 mm
$CTDI_{100,c}$	$CTDI_{100}$ measurements made at the centre of the phantom
$CTDI_{100,p}$	$CTDI_{100}$, represents an average of measurements at four different locations around the periphery of the phantom
${}_nCTDI$	CTDI measurements have been normalized to unit radiographic exposure (mAs)
${}_nCTDI_w$	Normalised weighted CTDI in the head or body phantom
DFOV	Display field of view
DLP_{air}	Dose length product free in air at the axis of the rotation
ERF	Edge response function
hPa	Hectopascal
HQ	High quality
HS	High speed
HU	Hounsfield unit
k_a	Air kerma length product
k_D	Air density correction
k_Q	Radiation quality correction
kg	Kilogram
kVp	Kilovolt (peak)

LIST OF ABBREVIATIONS (Continued)

Abbreviation	Term
lp/cm	Line pairs per centimeter
LSF	Line spread function
Gy.cm/C	Gray-centimeter per coulomb
mA, mAs	Milliampere, Milliampere-second
manSv	Mansievert
mGy, mGy.cm	Milligray, Milligray-centimeter
$mGy(mAs)^{-1}$	Milligray per milliampere-second
mm	Millimeter
mm^2	Square millimeter
MRI	Magnetic resonance imaging
mSv	Millisievert
MTF	Modulation transfer function
N_a	Ionization chamber calibration factor
N_a'	Calibration factor for air kerma length product, based on electrical units
Nt	The number of active data channels times the z-axis width of a single data channel
p	Air pressure
p_o	Reference value of air pressure (1013.2 hPa)
P, P'	Pitch for either a single-detector or multi-detector system
PSF	Point spread function
ROI	Region of interest
RPW	Radiation profile width
SD	Standard deviation
SFOV	Scan field of view
t	Temperature in Centigrade
T	The nominal scan width (FWHM of the section sensitivity profile)

LIST OF ABBREVIATIONS (Continued)

Abbreviation	Term
T_o	Reference value of temperature (293 K, 20 ^oC)
T’	The total nominal scan width along the z-axis for either a single-detector or multi-detector system

CHAPTER I
INTRODUCTION

Since its introduction into medical imaging, computed tomography (CT) has rapidly evolved in terms of both technical performance and clinical use. Over the past 25 years, CT has become the primary source of diagnostic radiation exposure. Most currently used x-ray CT scanners are the single-detector fan beam CT systems; however, the latest generation of CT with multi-detector systems has been a major leap forward in CT technology and will assure the future of the technique for many years to come (1).

Multi-detector CT is superior to single-detector CT for nearly all clinical applications. The superior speed of the former can be used to improve the temporal, spatial and contrast resolution of the images (2, 3). In addition, multi-detector CT shows promise for clinical applications that were limited or impossible with single-detector CT, such as cardiac imaging, organ perfusion studies and examinations of multiple vascular phases. Due to the technology advances, they have let to an explosive growth in the number of applications, to a capability of examining patients quickly and to a high rate of use.

On the other hand, however, the expanding use of multi-detector systems in clinical practice may result in a considerable increase in both the frequency of CT procedures and patient exposure levels. Accordingly data from various national surveys have confirmed, as a general pattern, the growing impact of CT as a major source of patient and population exposure (4). In addition, it is recognition that there is a potential risk of radiation that has driven many of the recent technical developments with CT and thus there is an increasing call to balance image quality against the risk. For these reasons, the following topics of multi-detector technology including image quality and radiation dose will be reviewed and discussed.

1.1 Multi-detector CT systems

The multi-detector (also known as multidetector-row or often used multi-slice) systems refers to a special CT system equipped with a detector array consisting of more than a single row of detectors. The first step in this direction was taken by different manufactures with so-called CT Twin or Dual-slice CT which has just two rows of detectors. This development led to a halving of any scan time, all other things being equal, since it may be seen as either acquiring two slices at a time or as covering twice the z-axis distance per rotation (1, 5).

Later the multi-detector systems with many more rows (16, 32, 40 to 64-row) were introduced following the development of 4-row detector technology. The advantages of the multi-detector system arise from its ability to acquire multiple sets of data in a single rotation, resulting either in four or more simultaneous axial images or four or more helical data sets. This means that one can either perform the same acquisition in a short time than with single-detector. Either perform a scan in the same time but with thinner slices, or scan a larger volume.

The benefits of multi-detector CT relative to single-detector CT are significant. The examination can perform with thinner sections, leading to higher spatial resolution along the longitudinal axis of the patient. Scanning can perform much faster, resulting in improve temporal resolution and reduce motion artifacts. Intravenously administer iodinate contrast material can deliver at a faster rate, increasing contrast enhancement in the images. These factors combine to improve the spatial, temporal and contrast resolution of the images, significantly increasing the diagnostic accuracy of the examination (2).

1.1.1 Detector array geometry

Multi-detector technique has been extended by several commercial companies. Three different detector array geometries are used by different manufactures (Figure 1). The detector array designs may be divided into two groups: those with detector elements of equal width along the z-axis (also called matrix detectors) and those with detector elements of unequal width (also called adaptive array detectors). GE Medical

Systems offers an equal-width detector array while Marconi, Siemens and Toshiba offer unequal-width detector arrays (1, 6)

The different geometries have an effect on the minimum slice thickness available and the number of slices available at this minimum width, the range of choice of slice thickness and the maximum volume/z-axis distance which may be scanned in any one system rotation (Table 1).

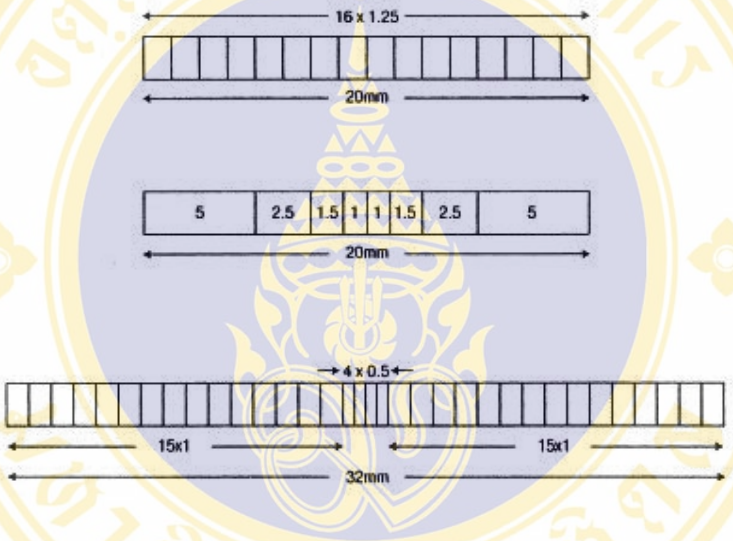

Figure 1. Profile of the various detector ring geometries used in the commercial systems. From top to bottom; (a) Consists of 16 identical detector rings (matrix array), (b) and (c) exploit ring detector widths of variable size. (Adaptive (b) and matrix/adaptive (c) arrays) (1).

Table 1. Comparison of various detector designs (1, 2).

Manufacturer	No. of elements	Detector widths (mm)	Slice width combination
GE	16	16 x 1.25	2 x 0.625, 4 x 1.25, 4 x 2.5, 4 x 3.75, 4 x 5, 2 x 10
Marconi/ Siemens	8	2 x 1.0, 2 x 1.5, 2 x 2.5, 2 x 5.0	4 x 0.5, 4 x 1, 4 x 2.5, 4 x 5, 2 x 8, 2 x 10
Toshiba	34	4 x 0.5, 30 x 1.0	4 x 1, 4 x 2, 4 x 3, 4 x 8

1.2 LightSpeed Plus CT scanner (7)

We performed experimental study on Lightspeed Plus CT scanner at radiology department, Ramathibodi Hospital. This multi-detector system is divided into sixteen 1.25-mm elements along the z-axis. The multi-detector system can image 20 mm of patient anatomy (referenced to the isocenter) as opposed to the 10-mm maximum coverage per x-ray exposure (in an axial mode) on the single-detector systems.

1.2.1 HiSpeed vs LightSpeed Plus (8) (Figure 2)

Single-detector row systems (such as GE HiSpeed) collimate the x-ray beam to the desired slice thickness and focus it on the center of the detector arc. Changing slice thickness is easy-simple open the collimator to increase the width of the x-ray beam. A single data set is acquired for each 360^{o} rotation of the x-ray tube.

With the LightSpeed matrix detector, the technology is much more complex. The x-ray beam is collimated to a wider thickness and focused on the central 4, central 8, central 12 or all 16 rows of detectors. Simultaneously, the data acquisition system selects which elements to acquire data from, using proprietary switching technology. For each 360^{o} rotation, four separate data sets are acquired.

Using the single-detector there can only be one slice per rotation. With the LightSpeed, there can be 1, 2 or 4 images per rotation. The results are better image quality with reduced partial volume artifacts at 1 image per rotation; and better image quality with 4 images per rotation.

Single-detector scanners gives 1 image every 2 seconds, and the LightSpeed gives up to 4 images every 2 seconds in axial mode, making the LightSpeed 4 times as fast. In helical mode, the LightSpeed can be up to 6 times fast.

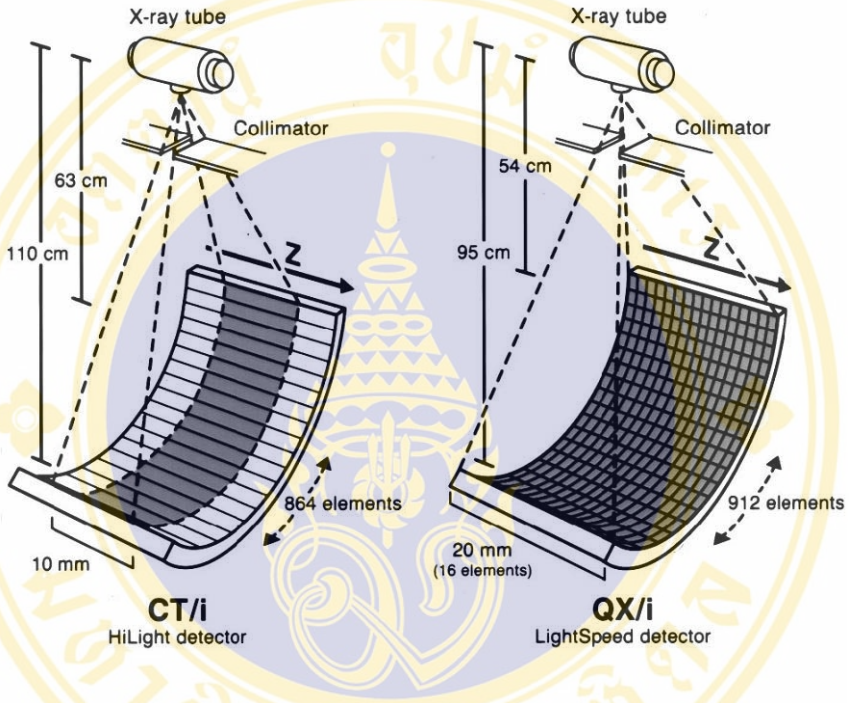

Figure 2. Illustration of the detectors used in a single-slice (GE HiSpeed CT/i) and multi-slice (GE LightSpeed QX/i) helical CT system. The detector dimensions along the *z*-axis are relative to the isocenter (e.g. the 20-mm depth of the LightSpeed detector is not the actual physical dimension of the detector, but rather the amount of *z*-axis coverage at the isocenter) (7).

1.2.2 Selection of slice thickness

One essential difference compared with conventional, single-row scanners is how slice thickness is generated. On a single-row scanner, slice thickness is achieved by a combination of primary and secondary collimation. Therefore the width of the detector array does not need to be limited. On multi-detector scanners, however, collimation can only be made for all detector rows together; slice thickness is merely determined by the width of the rows (9).

For imaging, the sixteen detectors can be configured in four ways, as shown in Figure 3. Data from one, two, three or four detectors are combined for each of four outgoing data channels.

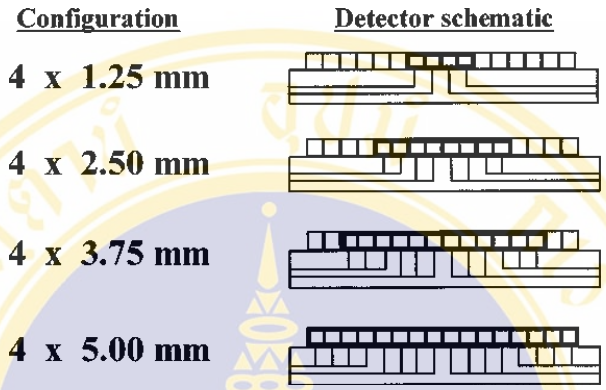

Figure 3. Illustration of the four detector configurations available on the multi-detector scanner. Four data acquisition channels are used to combine signals from one, two, three or four individual 1.25-mm detector elements. Once added together, the signal from an individual element cannot be recovered (7).

1.2.2.1 Axial imaging mode

In axial imaging, the user can choose both the number of images per rotation and the nominal image thickness, as shown in Table 2. In contrast to single-detector CT scanners, retrospective reconstruction of thinner or thicker scan widths is possible in the axial acquisition mode.

As an example, the four central rings may be selected to give a 4 x 1.25 mm simultaneous slice acquisition, or signals from pairs of configuration rings can be summed to allow 4 x 2.5 mm simultaneous slice acquisitions; summing the signals of three and four detector rings yields 4 x 3.75 and 4 x 5 mm simultaneous slice acquisitions, respectively.

By taking the signals of eight together (8 x 1.25 mm = 10 mm), on either side of the mid-line, 2 x 10 mm simultaneous slices may be obtained. Beam collimation allows the selection of half of each detector yielding a 2 x 0.625 mm slice acquisition (1).

Table 2. Axial imaging modes (7).

Detector configurations	Number of image per rotation		
	4	2	1
	Image thickness (mm)		
4 x 1.25 mm	1.25	2.5	5.0
4 x 2.5 mm	2.5	5.0	10.0
4 x 3.75 mm	3.75	7.5	-
4 x 5.0 mm	5.0	10.0	-
1 x 1.25 mm	-	-	1.25
2 x 0.625 mm	-	0.63	-

1.2.2.2 Helical imaging mode

The detector configuration choices for multi-detector helical imaging are the same as in the multi-slice axial mode; four channel each having a z-axis length of 1.25, 2.5, 3.75 or 5 mm, with a total active detector length of 5, 10, 15 or 20 mm, respectively (reference to the isocenter).

Pitch

The concept of pitch in spiral system has come to be understood. In single-detector helical system, pitch is defined as

$$P = \frac{Table\ \ travel\ \ per\ \ rotation}{T} \qquad (1)$$

where T equals the nominal scan width (i.e., the scan width specified by the operator, which is approximately equal to the full width at the half maximum of the section sensitivity profile) for one reconstructed image from the helical data set.

An alternative definition for the increased complexity of multi-detector CT, advocate a single definition of pitch, similar to that of Equation (1) is defined as

$$P' = \frac{Table\ \ travel\ \ per\ \ rotation}{T'} \qquad (2)$$

where T' equals the total nominal scan width along the z-axis for either a single- or multi-detector system.

In single-detector helical CT, the total nominal scan width *T'* along the z-axis remains equal to the nominal scan width *T* of one scan. In multi-detector helical CT, the total nominal scan width *T'* is equal to *Nt* (the number of active data channels times the z-axis width of a single data channel) and represents the total active detector width along the z-axis. For example, an $N = 4$ multi-detector scanner and a 5-mm data channel width, the total active detector width (total nominal scan width *T'*) is 20 mm. At a table speed of 15 mm per rotation, the pitch value computed using Equation (2) is 0.75, which is consistent with a 25% overlap of the radiation beam between consecutive rotations.

The multi-detector helical parameter choices available on the system tested are given in Table 3, the choice of two pitch values, which the manufacturer terms the high quality (HQ) or high speed (HS) modes of operation. The HQ mode operates at a helical pitch of 0.75 and the HS mode operates at a helical pitch of 1.5.

Table 3. Acquisition parameters for the HQ (high quality, pitch = 0.75) and HS (high speed, pitch = 1.5) helical imaging modes (7).

Detector configurations	Image thickness (mm)			Table travel (mm per rotation)	
				HQ	HS
4 x 1.25 mm	1.25	2.5		3.75	7.5
4 x 2.5 mm	2.5	3.75	5.0	7.5	15.0
4 x 3.75 mm	3.75*	5.0	7.5	11.25	22.5
4 x 5.0 mm	5.0	7.5	10.0	15.0	30.0

*3.75-mm thickness not available at 22.5 mm/rotation

1.2.3 Clinical applications (2, 6, 10, 11)

One of the main benefits of multi-detector CT systems is their capability to cover a body length with narrow slice widths. This is made possible because the acquisition of many simultaneous slices increases the efficiency with which the x-ray tube heat capacity is utilized**.** It also helps decrease the total examination time. Additionally, imaging with narrow slices has great diagnostic advantages.

A combination of the multiple detector rows and faster gantry rotation times allows applications such as CT myelography, CT angiography, virtual endoscopy, musculoskeletal applications, brain perfusion and cardiac imaging. Phase selective imaging after intravenous contrast enhancement for various organ systems, especially hepatic imaging is also possible.

In trans-axial images partial volume artifact is reduced**,** and contrast differences can be increased. The improved image quality in MPR (multi-planar reconstruction) and 3-D reconstructions is particularly notable. Whole body coverage with 1 mm slices is now feasible. Routine multi-detector CT with 0.5 - 2 mm slices means that for the first time CT can be regarded as an isotropic imaging modality, i.e., providing images with a similar spatial resolution in all three dimensions. Data can now be viewed in all planes with image quality almost the same as, if not better than, that of a trans-axial image.

Other major advantages of multi-detector CT are higher patient comfort in the form of shorter and fewer breath-holds in body imaging, avoiding awkward positioning for coronal imaging and minimizing sedation for pediatric patients. Critically ill patients can also be scanned much faster.

1.3 Radiation dose

1.3.1 Patient dose in multi-detector CT

Since the introduction of multi-detector CT scanner, multi-detector technology increases the efficacy of CT procedures and offers new promising applications. The expanding use of multi-detector CT, however, may result in an increase in both frequency of procedures and level of patient exposure. Therefore the question arises whether the introduction of multi-detector CT is associated with a reduction or an

increase in patient exposure in practice. The most interesting question was how multi-detector CT exposure compares with single-detector CT practice.

To answer this question, the first paper was published in 1999 (7). This studied was to characterize the performance of a recently introduced multi-detector CT (LightSpeed QX/i) in comparison to a single-row scanner (HiSpeed CT/i) from the same manufacturer (GE Medical Systems). By focus on dose the results were stated that the computed tomography dose index (CTDI) of multi-detector system was provided at varying degrees of increased dose relative to the single-detector scanner. Other studied in 2000 by Kalender (12) was able to show that on the basis of equivalent scanning parameters dose from spiral scanning are broadly similar to those from serial scanning although increased by 10 - 30% will occur with multi-detector scanners. Similar results were obtained by Brix et al. (13) with studied to gain an overview of multi-detector CT examinations conduced in Germany in 2001. Then the results were compared with those previous surveys for single-detector scanners. With the average effective dose to patients was changed from 7.4 mSv at single-detector to 8.1 mSv at multi-detector scanners

All of them reported on a significant increase in patient dose following the introduction of multi-detector CT technology. Furthermore, it is probable that the overall dose burden to the population will increase with the greater range of scanning capabilities now available. According to surveys conducted at United States medical facilities, the annual number of CT examinations increased from approximately 3.6 million in 1980, to 13.3 million in 1990, and to 33 million in 1998 (14). A recent paper from USA indicates that in a department with typical referral pattern CT scans now constitute 11% of the examinations and contribute 67% of the collective dose (15). Similarly, in UK the contribution of CT to the annual population dose from medical radiation exposures was estimated at 20% in 1990, rising 40% in 1999 (16). In addition, several national surveys have been concluded that CT contributes to more than 50% of the collective dose from the medical use of radiation to day (4).

1.3.2 Why is multi-detector CT a high dose examination?

There are any dose disadvantages associated with multi-detector scanning. Then there is a geometrical efficiency decrease associated with the inter-detector gaps and the fact that greater scatter is associated with cone beams. Moreover, the increased use of narrow slices may lead to higher doses for two reasons. Firstly, a higher tube current is needed to keep image noise to an acceptable level, though possibly not to the extent one might expect because of the improved contrast achieved due to less partial volume effect with thin slices. Secondly, the beam penumbra contributes a significant additional dose on 4-row detector scanner used with narrow collimations as known as over beaming (3).

1.3.3 CT dosimetry

Because of its geometry and usage (17), the conditions of exposure during CT examinations are quite different from in conventional x-ray procedures and specific techniques are necessary in order to allow detailed assessment of patient dose from CT (18, 19). Reference dose quantities are discussed below.

Dose quantities for CT (18, 20)

1.3.3.1 Computed Tomography Dose Index (CTDI)

The principal dosimetric quantity used in CT is the *computed tomography dose index (CTDI)*. This is defined (21) as the integral along a line parallel to the axis of rotation *(z)* of the dose profile *(D(z))* for a single slice, divided by the nominal slice thickness T:

$$CTDI = \frac{1}{T}\int_{-\infty}^{+\infty} D(z)dz \qquad (mGy) \qquad (3)$$

In practice, a convenient assessment of CTDI can be made using a pencil ionization chamber with an active length of 100 mm so as to provide a measurement of $CTDI_{100}$ expressed in terms of absorbed dose to air (mGy). Such measurements may be carried out free-in-air on or parallel with the axis of rotation of the scanner $(CTDI_{100,\,air})$, or at the centre $(CTDI_{100,\,c})$ and 10 mm below the surface $(CTDI_{100,\,p})$ of standard CT dosimetry phantoms. The subscript `n' $({}_nCTDI)$ is used to denote when these measurements have been normalised to unit radiographic exposure (mAs).

Such measurements of CTDI in the standard head or body CT dosimetry phantom may be used to provide an indication of the average dose over a single slice for each setting of nominal slice thickness. On the assumption that dose in a particular phantom decreases linearly with radial position from the surface to the centre, and then the normalised average dose to the slice (22) is approximated by the (normalised) weighted CTDI *($CTDI_w$)*:

$$ {}_nCTDI_w = \frac{1}{C}\left(1/3CTDI_{100,c} + 2/3CTDI_{100,p}\right) \qquad (mGy(mAs)^{-1}) \qquad (4) $$

where C is the radiographic exposure (mAs), $CTDI_{100,c}$ represents a measure at the center of the dosimetric phantom and $CTDI_{100,p}$ represents an average of measurements at four different locations around the periphery of the phantom. Values of ${}_nCTDI_w$ can vary with nominal slice thickness, particularly for the narrowest settings.

1.3.3.2 Reference dose quantities

Two reference dose quantities are proposed for CT in order to promote the use of good technique:

(a) Weighted CTDI in the standard head or body CT dosimetry phantom for a single slice in serial scanning or per rotation in helical scanning:

$$ CTDI_w = {}_nCTDI_w \cdot C \qquad (mGy) \qquad (5) $$

where ${}_nCTDI_w$ is the normalised weighted CTDI in the head or body phantom for the settings of nominal slice thickness and applied potential used for an examination (Equation 4) and C is the radiographic exposure (mAs) for a single slice in serial scanning or per rotation in helical scanning.

Monitoring of $CTDI_w$ for the head or body CT dosimetry phantom, as appropriate to the type of examination, provides control on the selection of exposure settings, such as mAs.

(b) Dose-length product for a complete examination:

$$ DLP_{Axial} = \sum_i nCTDI_w \cdot T \cdot N \cdot C \qquad (mGy\ cm) \qquad (6) $$

where i represents each serial scan sequence forming part of an examination and N is the number of slices, each of thickness T (cm) and radiographic exposure C (mAs), in

a particular sequence. Any variations in applied potential setting during the examination will require corresponding changes in the value of ${}_nCTDI_w$ used.

In the case of helical (spiral) scanning:

$$DLP_{Helical} = \sum_i nCTDI_w \cdot T \cdot A \cdot t \qquad (mGy\ cm) \qquad (7)$$

where, for each of i helical sequences forming part of an examination, T is the nominal irradiated slice thickness (cm), A is the tube current (mA) and t is the total acquisition time (s) for the sequence. ${}_nCTDI_w$ is determined for a single slice as in serial scanning.

Monitoring of DLP provides control on the volume of irradiation and overall exposure for an examination.

Such measurements may be carried out free-in-air on or parallel with the axis of rotation of the scanner, simply named $CTDI_{air}$ or DLP_{air}. Dose free-in-air has up to now been the most important dose quantity for CT in Germany. It is also used more widely; however, $CTDI_{air}$ is not well-suited for use as a reference dose quantity since the setting of a single level for a given procedure would not equitably dictate practice for all scan types of scanner. $CTDI_{air}$ can, however, still be an important element in the implementation of patient dosimetry (20).

1.4 Image quality

Image quality is a function of dose and can be quantified by three basic concepts that are contrast resolution, spatial resolution or clarity and noise.

1.4.1 Spatial resolution (23, 24)

Spatial resolution is a common parameter used to evaluation of imaging systems. It characterizes the imaging system's ability to distinguish between two very small objects placed closely together. The point between two small objects with very different densities is considered to be a region of high frequency or high contrast. Spatial resolution measurements are performed with objects which have a high contrast (contrast difference of 12% or greater) from uniform background.

Several methods that quantify or measure spatial resolution include the point spread function (PSF), line spread function (LSF), edge response function (ERF) and the modular transfer function (MTF). The MTF is the most commonly used method to measure the spatial resolution capabilities of a CT system, which is graphically depicted.

The MTF demonstrates the frequency components of a structure in line pairs per centimeter (lp/cm) as shown in Figure 4. In this figure, optical density is used to express the image fidelity, the faithfulness with which the object can be reproduced in the image. A line pair phantom consists of line pair pattern that are placed at different widths apart. This means if more lines that can be visualized separate from one another, the better the systems spatial resolution.

Spatial resolution depends upon imaging high frequency structures located a very small distance apart. An MTF value of 1.0 represents a complete, without blurring, transfer of an object through the CT system to a monitor. An MTF value of 1.0 corresponds to imaging large structures that can very easily be imaged accurately by most CT systems. Therefore, the value of 0.1, which represents small, high frequency or density structures, is used to evaluate the spatial resolution capabilities of a CT system. The more lp/cm a CT system produces, the better the spatial resolution. In Figure 4, at 1 line pair (lp)/cm spatial frequency, the optical density is 0.88 at 2 lp/cm, the optical density is 0.59 and so on.

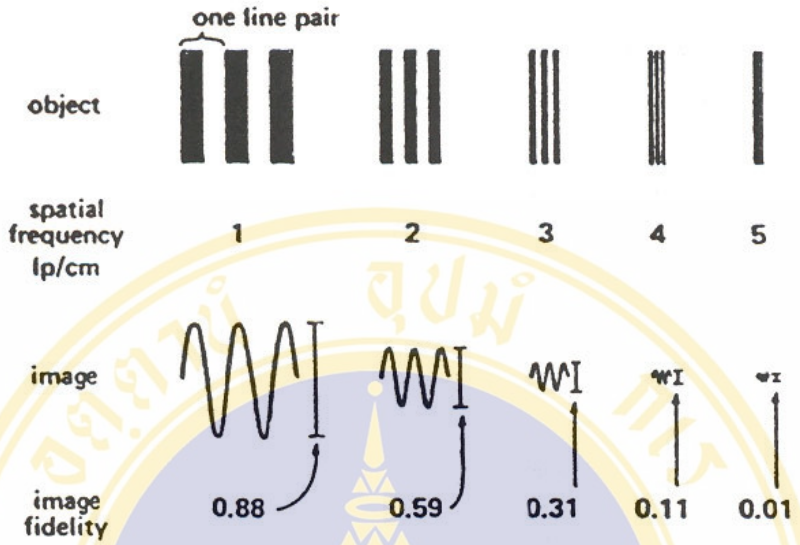

Figure 4. A bar pattern (object) consists of line pair (lp, where one line pair is equal to one bar plus one space), where the number of line pairs per unit length is called the spatial frequency. Large objects have a low spatial frequency whereas small objects have a high spatial frequency (23).

If the spatial frequency is plotted as a function of the image fidelity, an MTF curve is obtained (Figure 5). The MTF curves for two CT scanners are given in Figure 6. It can be seen that scanner A can image 5.2 lp/cm at 0.1 MTF compared with scanner B, which can only image 3.5 lp/cm at 0.1 MTF. This simply means that scanner A has a better spatial resolution capability than scanner B. Or scanner A is capable of separating smaller objects than scanner B because the structures edges will be less blurred.

High contrast spatial resolution is influenced by factors including: system geometric resolution limits-focal spot size, detector width and ray sampling, pixel size and properties of the convolution kernel/mathematical reconstruction filter (25).

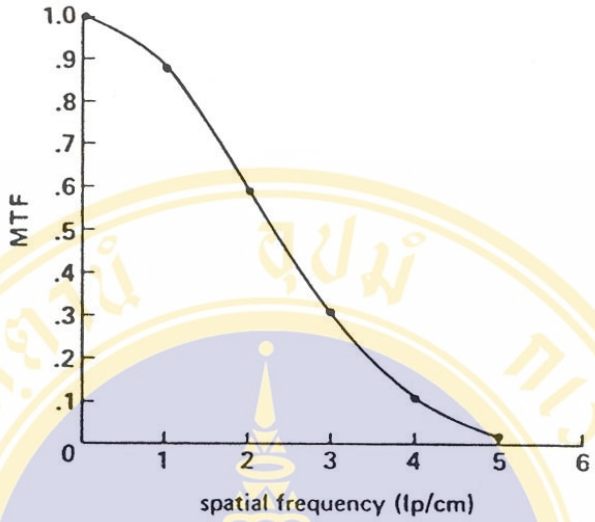

Figure 5. MTF (Modulation Transfer Function) curve obtained from the data given in Figure 4 (23).

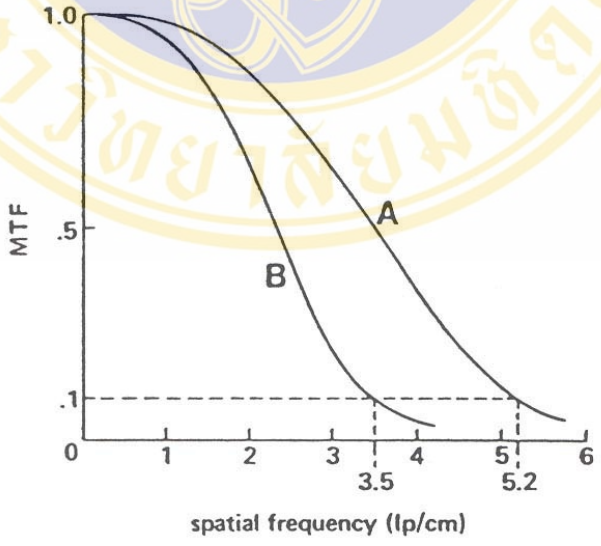

Figure 6. MTF curves for two CT scanners (23).

1.4.2 Noise (24)

Noise is considered to be the number one limiting factor of CT image quality. Noise is the portion of a signal that contains no information that characterized by a grainy appearance of the image. Many authors describe noise as a salt and pepper pattern on the CT image. If a quality assurance phantom is comprised of a known material like water, when the phantom is used to evaluate the quality of image, it is expected that every portion of that phantom would have the CT number zero. Due to the statistical fluctuation in every scan it is impossible for this to occur. The level of noise in an image is recorded as the standard deviation in an ROI measurement. The larger the standard deviation, the less accurate the average CT number of the ROI.

Noise is a parameter showing the intrinsic lack of uniformity in the image and it is mainly due to the quantum structure of the radiation interacting with the detector, or to the fact that the number of photons, incident locally on a generic area, varies statistically. Moreover it is also caused by factors intrinsic to the system, such as structural variability, electronic noise, etc. Noise influences mainly the possible to detect the details at low contrast, when the object tends to fade into the fluctuations of signal.

Image noise is influenced by a large number of parameters, including: kVp, mA, exposure time, collimation/reconstructed slice thickness, reconstruction algorithm or filter, helical pitch/table speed, helical interpolation algorithm or others (focal spot to isocenter distance, detector efficiency, etc.) (25).

1.4.3 Contrast resolution (24)

Contrast resolution is the ability of a CT scanner to differentiate small attenuation differences on the CT image. Contrast is also known as low contrast resolution and tissue resolution. CT can image tissues that vary only slightly in density and atomic number. Most soft tissues have atomic numbers or densities that are nearly the same. The ability of the CT scanner to image these slight differences is knows as low contrast detectability, which is used to describe contrast resolution in CT. Low contrast resolution is typically evaluated with a phantom that contains low contrast objects of varying sizes.

Contrast resolution is limited by noise, as noise in an image increases; contrast resolution decreases thereby, inhibiting the ability of the CT scanner to image slight differences in tissue density.

Low contrast resolution is influenced by a large number of factors that include a similar list to that described above for image noise. In addition, the actual test results can also be influenced by factors such as window and level settings, the monitor or film calibration curve and the observer themselves (25).

1.5 Factors affecting image quality and dose (26)

Imaging parameters such as x-ray tube voltage, current and rotation time, as well as the table speed and imaging mode are important factors in the determining how much radiation will be administered to a patient. These factors are controlled by the user at the time of CT. The influence of changes in some key technical and operational parameters on image quality and patient dose are discussed below (focus on the experimental study parameters).

1.5.1 Typical CT scan parameters

1.5.1.1 Nominal slice thickness

The nominal slice thickness in CT is defined as the full width at half maximum (FWHM) of the sensitivity profile, in the centre of the scan field; its value can be selected by the operator according to the clinical requirement and generally lies in the range between 1mm and 10mm. In general the larger the slice thickness, the greater the low contrast resolution in the image; the smaller the slice thickness, the greater the spatial resolution. If the slice thickness is large, the images can be affected by artifact, due to partial volume effects; if the slice thickness is small (e.g. 1-2mm), the images may be significantly affected by noise.

1.5.1.2 Inter-slice distance/ pitch factor

Inter-slice distance is defined as the couch increment minus nominal slice thickness. In helical CT the pitch factor is the ratio of the couch increment per rotation to the nominal slice thickness at the axis of rotation. In clinical practice the inter-slice

distance generally lies in the range between 0 and 10mm, and the pitch factor between 1 and 2. The inter-slice distance can be negative for overlapping scans which in helical CT means a pitch < 1. In general, for a constant volume of investigation, the smaller the inter-slice distance or pitch factor, the higher both the local dose and the integral dose to the patient. The increase in the local dose is due to superimposition of the dose profiles of the adjacent slices. The increase in the integral dose is due to an increase in the volume of tissue undergoing direct irradiation as indicated by a packing factor.

In those cases where 3D reconstruction or reformatting of the images in coronal, sagittal or oblique planes is required, it is necessary to reduce the inter-slice distance to zero or perform a helical scan. In screening or examinations performed with regard to control of disease it can be diagnostically justifiable to have an inter-slice distance corresponding to half the slice thickness or a pitch factor of 1.5 - 2.

1.5.1.3 Exposure factor

Exposure factors are defined as the settings of x-ray tube voltage (kV), tube current (mA) and exposure time (s). In general, one to three values of tube voltage (in the range between 80 and 140 kV) can be selected. A high tube voltage is recommended for high resolution CT (HRCT) of the lungs and may be used for examination of osseous structures such as the spine, pelvis and shoulder. Soft tissue structures are usually best visualized using the standard tube voltage for the given equipment. In some cases of quantitative computed tomography (QCT), the same slice is examined with two different values of tube voltage, in order to subtract corresponding images and derive information about the composition of particular tissues.

At given values of tube voltage and slice thickness, the image quality depends on the product of x-ray tube current (mA) and exposure time (s), expressed in mAs. Absolute values of mAs necessary for an imaging task will depend on the type of scanner and the patient size and composition. For a particular CT model, an increase in radiographic exposure setting (mAs) is accompanied by a proportional increase in the dose to the patient. Relatively high values of radiographic exposure

setting (mAs) should therefore be selected only in those cases where a high signal to noise ratio is indispensable.

A method for correlating the exposure setting (for a given tube voltage) with the overall image quality is by drawing contrast-detail curves for each available setting. These curves express the minimum size of detail which can still be recognized in the CT image for a given difference in contrast between the detail and the surrounding medium.

1.5.1.4 Field of view

Field of view (FOV) is defined as the maximum diameter of the reconstructed image. Its value can be selected by the operator and generally lies in the range between 12 and 50 cm. The choice of a small FOV allows increased spatial resolution in the image, because the whole reconstruction matrix is used for a smaller region than is the case with a larger FOV; this results in reduction of the pixel size.

Pixel size is a factor that influences spatial resolution which is influenced by the chosen, scanned field of view (SFOV) and matrix size:

$$Pixel\ \ size = \frac{FOV}{matrix\ \ size} \tag{8}$$

where matrix size is the array of rows and columns of pixels in the reconstructed image, typically 512 x 512.

In any case, the selection of the FOV must take into account not only the opportunity for increasing the spatial resolution but also the need for examining all the areas of possible disease. If the FOV is too small, relevant areas may be excluded from the visible image. If raw data are available the FOV can be changed by post processing.

1.5.2 Multi-detector scan parameters

The CT LightSpeed Plus scanner system provides more options and involves manipulating a variety of CT parameters such as; kVp: 80, 100, 120 and 140, scan speed: full 360^{o} rotational scans in 0.5, 0.6, 0.7, 0.8, 0.9, 1.0, 2.0, 3.0 and 4.0 seconds, mA: 10 to 440 mA with 10 mA increments, scan field of view: 25 cm for adult head, 25, 50 cm for body and 25 cm for pediatric head, pitch: 0.75 and 1.5. More slice

thickness are acquire, as discussed in the topic of selection of slice thickness, image thickness is selected by changing collimation, detector configuration and reconstruction algorithm.

1.6 Optimization process

Although from this technology, there have been several important consequences. First, there are more options (and therefore protocols) for CT evaluation. These options involve manipulating a variety of CT parameters that control the amount of radiation delivered, a direct determinant of image quality (17). While there are many options, some of these are inappropriate in that the amount of radiation a patient receives is in excess of what is necessary for obtaining a diagnostic examination (27). Thus, there is a considerable potential for dose reduction at multi-detector systems by an optimization of scan protocols.

First, sufficient justification should be made for each CT examination performed. The CT examination should be performed only when appropriate. If a modality such as MRI, ultrasound or sonography can provide sufficient information, the risk of radiation should be avoided altogether.

Then in an optimization process, good imaging performance demand that image quality should be sufficient to meet the clinical requirement for the examination, whilst maintaining the dose to the patient at the lowest level that is reasonably practicable (ALARA) (27, 28). By the quality of the image relates to the fidelity of the CT numbers and to the accurate reproduction of mall differences in attenuation (low contrast resolution) and fine detail (spatial resolution) (26). Patient dose can only be reduced to levels at which the detectability of relevant details is not unduly affected by increased noise (spatial resolution is less subject to noise than those of only low contrast) (29).

In order to achieve this, one must be careful selection of technical parameters that control exposure of the patient and the display of images. CT radiation dose optimization based on modification of scanning parameters is the method that most useful strategy in practical and used in this study. This study, scan parameters such as tube current (mA), slice thickness, pixel size and pitch (in helical mode) of a multi-

detector CT were varied and used these varied protocols as the guidelines for dose optimization.

CHAPTER II
OBJECTIVES

The main objective of this study was to investigate optimized scanning parameters for different scanning protocol used in multi-detector CT at Ramathibodi Hospital.

The sub-objectives of this study were:

1. To characterize performances of a multi-detector CT unit in term of image quality and radiation dose as a function of various scanning parameters.

2. To select optimized scan parameters so that the optimal dose level to patients will be achieved.

The expected results from this study are guidelines for setting up clinical imaging protocols suitable for each diagnostic CT investigation in terms of minimizing radiation dose while maintaining acceptable image quality.

CHAPTER III
LITERATURE REVIEWS

Research on dose reduction must, therefore, focus on image quality and standard practice. The challenge to practitioners is to identify acceptable thresholds of image quality so that the minimum radiation doses needs to achieve these can be determined. Reduction in tube current is the most practical means of reducing CT radiation dose. Authors of previous studies (30-33) on CT of the head, sinus, chest and pediatric have suggested that it is possible to reduce tube current without markedly affecting image quality.

Paper of CT dose optimization was studied by Crawley et al (34). The studied was done from following the installation of a helical CT scanner (Siemens Somatom Plus 4) over a period of about 2 years. CT scan parameters in this hospital (Stoke Mandeville Hospital, UK) have been adjusted by optimum selection of technique factors (tube current (mA) and/or rotation time were the gradually reduced and slice width and/or pitch were gradually adjusted). And after adjustment of clinical scan protocols, a 33% reduction in annual collective effective dose has been achieved, from about 16.5 manSv to 11 manSv.

While the previous studies of CT dose optimization are usually performing in a conventional CT (spiral or single-row CT). Understanding patient radiation exposure, or dose, in conventional radiography and single-detector is relatively straightforward, but the same cannot be said of multi-detector CT. Multi-detector CT is complex and more options, consequently the knowledge of scanning technique (mAs and kVp) and factors such as slice thickness, pitch and differences in system design are essential to an understanding of multi-detector CT dose.

Dose characteristics of multi-detector CT were studied by Hamberg et al (35). Weighted CT dose index ($CTDI_{100w}$) values were obtained from three multi-detector CT scanners (LightSpeed; GE medical Systems) for both head and body CT modes by using standard CT dose phantoms. The $CTDI_{100w}$ was determined as a function of x-ray tube voltage (80, 100, 120, 140 kVp), tube current (range, 50 - 380 mA), tube rotation time (0.5 - 4.0 seconds), radiation profile width (RPW) (5, 10, 15, 20 mm) and acquisition mode (helical high quality and high speed modes and axial one-, two- and four-section modes). In summary, the $CTDI_{100w}$ increased in linear with tube current and tube rotation time and thus with the milliampere second value. In all scanning modes, $CTDI_{100w}$ decreased when RPW increased.

Koller et al (36) studied the variations in radiation dose between the same models of multi-detector CT scanner at different hospitals. With the variation in exposure factors and patient dose between seven centers was investigated for six standard examinations. Dose values were compared with each other and the relevant diagnostic reference level (DRL) for each examination. The range in weighted CT dose index ($CTDI_w$) values between the seven centers was small for abdominal and head scans. For other scans however, such as functional endoscopic sinonasal surgery (FESS) the variations in $CTDI_w$ was as high as a factor of seven between the lowest and the highest values. And at one hospital where dose optimization has been implemented, this center had $CTDI_w$ values ranging from 3% to 64% lower than the average value for the seven centers whilst maintaining diagnostic image quality.

This study has shown a considerable variation in the choice of user-selectable exposure factors for some common types of examination, carried out on the same model of CT scanner, at a number of different hospitals. The resulting variation in CT dose was due to the variation in user-selectable exposure alone.

In multi-detector CT dose optimization, many studies in patient and/or phantom have been performed to determine the possibility of reducing CT radiation doses for specific clinical indications as some example from the following studied.

Prasad et al (37) have reported that chest CT image quality appears to be acceptable for evaluating normal anatomic structures even with a 50% reduction in radiation dose. In addition, low dose multi-slice CT has been recommended for screening for lung cancer (38). Macari et al (39) reported that low dose multi-detector

CT colonography has excellent sensitivity and specificity for detection of colorectal neoplasms 10 mm and larger. Spielmann et al (40) used an anthropomorphic torso phantom and reported unimpaired visualization of renal calculi on images obtained with markedly reduced tube current on single-detector and multi-detector CT scanners, with a dose reduction of more than 75%.

In addition, tube current can be reduced on the basis of patient weight as the studied by Kalra et al (41). The quality of abdominal CT images obtained with a multi-detector CT at a 50% reduced radiation dose was compared with that of images obtained with a standard dose. Although standard dose images were less noisy and more visually pleasing in patients weighting less than 81.6 kg, image quality at 50% reduced tube current was acceptable. In contrast, for patients weighting more than 81.6 kg, reduced dose CT images were found to be too noisy, and image quality was not acceptable. It follows that lighter patients should be evaluated with reduced radiation by changing the tube current according to the patient's weight.

From the knowledge of all previous studies that are discussed above lead to this research study on dose optimization. While mostly dose optimization in multi-detector CT in previous studies were mainly focused on reduction in tube current (mA) but multi-detector CT can perform with variety of selection scan parameters; therefore, in the present study not only tube current (mA) but also other scan parameters such as slice thickness, pixel size and pitch were used to consider.

CHAPTER IV
MATERIALS AND METHODS

This study was performed on a multi-detector CT scanner. Various imaging parameter combinations, i.e., tube current (mA), slice thickness, pixel size and pitch (in helical mode) were selected to assess image quality (spatial resolution, low contrast resolution and noise) and dose (dose length product, DLP_{air}).

4.1 Materials

4.1.1 Multi-detector CT (MDCT) scanner (42)

The multi-detector row CT system (LightSpeed Plus, GE Medical Systems, Department of Radiology, Queen Sirikit Medical Center, Ramathibodi Hospital) used in this study was a 4-detector row scanner.

4.1.2 Phantoms

Two types of quality control phantoms were employed in this study.

4.1.2.1 A quality assurance phantom (QA phantom) (42) (Figure 7-a)

This phantom (21.5 cm diameter) contains three sections, each corresponding to a single scan plane.

Section 1 Resolution block

Section 1 of the phantom contains six sets of bar patterns in a plexiglass block used to test high contrast spatial resolution. Each pattern consists of sets of equally sized bars and spaces. Water fills the spaces and provides about 12% (120 HU) contrast. The resolution block contains the following bar sizes 1.6 mm, 1.3 mm, 1.0 mm, 0.8 mm, 0.6 mm and 0.5 mm.

Section 2 Contrast membrane

Section 2 of the QA phantom is used to test low contrast detectability, defined here as the smallest hole size visible for a given contrast level at a given dose. This phantom section contains a doped polystyrene membrane suspended in water and pierced by a series of holes in the following sizes 10.0 mm, 7.5 mm, 5.0 mm, 3.0 mm and 1.0 mm.

Section 3 Water bath

Section 3 of the phantom is used to test noise and uniformity, QA phantom section 3 provides a uniform image by which to assess image CT number noise and uniformity.

4.1.2.2 A resolution phantom (43) (Figure 7-b)

This phantom is used to measure both high and low contrast resolution as well as slice thickness and the scanner's contrast scale.

a. b.

Figure 7. Phantoms used in this study: (a) QA phantom, (b) resolution phantom.

4.1.3 Dosimeter (44)

A NOMEX dosimeter (Figure 8-a) type L981603, PTW-FREIBURG for acceptance tests and quality assurance of diagnostic x-ray equipment. The PTW-NOMEX features an input channel for dose and dose rate measurements as well as two input channels for the determination of the tube voltage, the exposure time and the mAs product. The input channel for dose and dose rate measurements accepts also a long cylindrical chamber for the measurement of the dose length product on CT units. The measurement range for the dose length product is 100 mGy.cm - 999.9 mGy.cm with a digital resolution of 0.1 mGy.cm in the smallest range.

4.1.4 Ionization chamber (45)

A cylindrical ionization chamber (Figure 8-b) type/Ser.-No. M30009-0222, PTW-FREIBURG for the measurement of photon radiation in computed tomography. The chamber has an effective length of 100 mm, 0.9 cm outer diameter and a measuring volume of 3.14 cm^3. Nominal useful range 70 - 150 kV.

4.1.5 Spirit level

4.1.6 Thermometer and Barometer

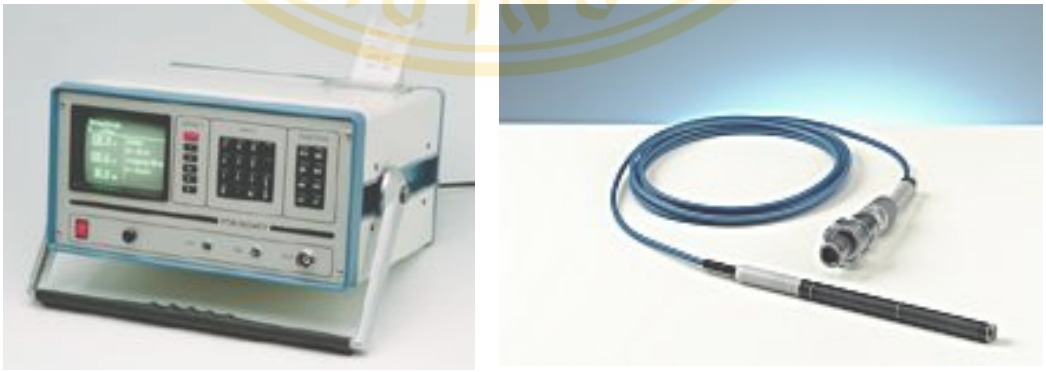

a. b.

Figure 8. (a) A NOMEX dosimeter, (b) A pencil chamber (PTW, Frieburg)

4.2 Methods

4.2.1 Image quality and radiation dose reproducibility

To ensure the quality of the CT machine throughout the period of this experimental study, reproducibility tests on radiation output and image quality in terms of noise and image uniformity were performed (see Appendix).

4.2.2 Data acquisition protocols

In our study, to assess the optimal scanning parameters, the mA, slice thickness, pixel size and pitch (in helical mode) were varied from the routine techniques (Table 4). Sets of data acquisition protocols were selected from head and abdomen protocols.

There were two main parts of the scanning protocols; head (routine head protocol) and body (upper abdomen protocol). The two main protocols were then subdivided into two parts; posterior fossa and above posterior fossa in head, pre-contrast and post-contrast in body, respectively.

For head scan protocols the axial mode was employed, examinations were performed with 2 second scan time, the mA setting was varied from 100 to 160 mA with the increment steps of 5 mA each time. Large (50 cm) and small (25 cm) scan field of view (SFOV) were used with the same displayed field of view (DFOV) 20 cm with corresponding 0.98 and 0.49 mm pixel size, respectively. The slice thickness was varied from 1.25 to 10.00 mm.

For body scan protocols, the helical mode was employed, examinations were performed with 0.8 second rotation time, pitch settings of 0.75 (high quality, HQ) and 1.5 (high speed, HS), the mA setting varied from 140 to 240 mA with the increment steps of 10 mA. Large (50 cm) and small (25 cm) SFOV were used with 35 cm and 25 cm DFOV, with corresponding 0.98 and 0.49 mm pixel size, respectively. Slice thickness were ranged from 1.25 to 10.00 mm, beam collimation ranged from 1.25 to 5.00 mm and table speed ranged from 3.75 to 30.00 mm per rotation.

All measurements were performed by using 120 kV, 512 x 512 matrix size and standard reconstruction algorithm.

Variation of scan parameters in the study of radiation dose was slightly different from the study of image quality due to differences in the subdivided parts and scan length in each slice thickness. These differences will be shown in tables of chapter 5.

Table 4. CT scan parameters in Ramathibodi Hospital.

	Images	Scan type	Start location	End location	No. of image	Thick speed	Interval (mm)	SFOV DFOV	kV	mA
Routine Head										
Pre contrast	1-20*	Axial Full 2 sec	S 0	S 47.5	20	2.5(2i)	5	Head/ 20 cm	120	160
	21-30**	Axial Full 2 sec	S 50	S117.5	10	7.5(2i)	15	Head/ 20 cm	120	140
Post contrast	1-20*	Axial Full 2 sec	S 0	S 47.5	20	2.5(2i)	5	Head/ 20 cm	120	160
	21-30**	Axial Full 2 sec	S 50	S 117.5	10	7.5(2i)	15	Head/ 20 cm	120	120
Upper Abdomen										
Pre contrast	1-31	Helical Full 1 sec	S 50	I 250	31	10.0 15.00 1.75:1	10	Large/ 30 cm	120	200
Post contrast	1-40	Helical Full 0.8 sec	S 0	I 146.25	40	3.75 11.25 0.75:1	3.75	Large/ 36 cm	120	220
	41-80	Helical Full 0.8 sec	S 0	I 146.25	40	3.75 11.25 0.75:1	3.75	Large/ 36 cm	120	220

*posterior fossa, **above posterior fossa

4.2.3 Phantom scan

The phantom was positioned and properly leveled on the phantom holder or the couch. The laser alignment light was used to position the phantom (Figure 9). The longitudinal and transverse surfaces of the phantom were aligned parallel to the scanner axis and the tomographic plane, respectively. The scanner axis and the tomographic plane must coincide with the longitudinal axis of the phantom and with the center of phantom length, respectively.

Check the phantom alignment and quite generous tolerance were allowed for the set up: 2 degrees for left to right through the vertical plane and tilt from the horizontal, 5 mm for lateral and vertical displacements (46). Scan the phantom by varying scan parameters from the routine setting

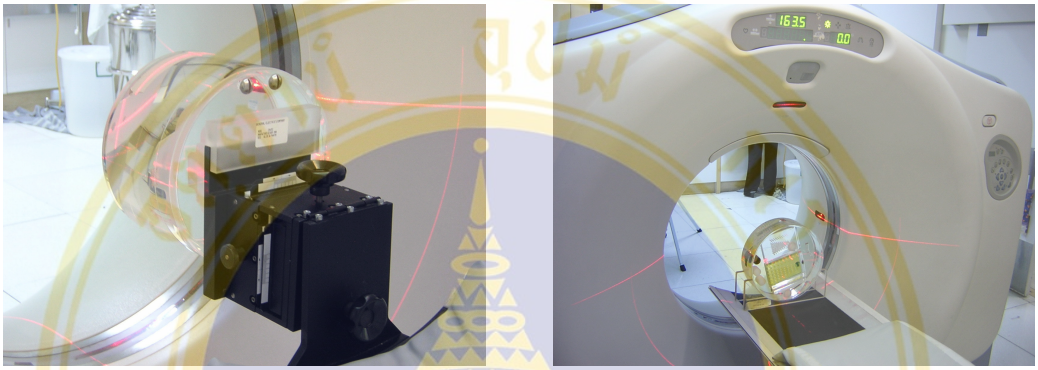

a. b.

Figure 9. Phantom positioning and alignment: (a) QA phantom is place on the phantom holder, (b) resolution phantom is place on the couch.

4.2.4 Dose measurement

To evaluate the exposure to patients for the whole examination, dose length product (DLP) measurements were made free-in-air with the ionization chamber on the scanner central axis.

The ionization chamber was placed at the isocenter of the scanner with its axis aligned to the axis of rotation. The position of the chamber was checked by performing a scan or by using of the laser pointers of the scanner (Figure 10). The chamber was positioned so that it extended beyond the end of the table in order to exclude attenuation of beam by the table. The axis of the chamber was also perpendicular to the tomographic plane, and the marker at the center of the chamber length was coincided with the center of the fan beam. The chamber alignment was checked the same way as the procedures in phantom alignment.

To carry out the measurements, temperature and pressure were measured and recorded. At the beginning of the measurements 3 exposure readings were taken, if

the readings were constant (< 3% variation) it may be possible to save time by making only one exposure for subsequent studies (46).

Figure 10. Chamber positioning and alignment: free-in-air with the chamber on the axis of rotation.

4.2.5 Image quality assessment

For evaluating the spatial resolution, low contrast resolution and image noise, only the first image of each examination was used and displayed on the image monitor of a CT scanner. Window width, window level and image zoom were set appropriately for visualization and keep constant for each image quality evaluation.

4.2.5.1 Spatial resolution

High contrast spatial resolution is described as the minimum distance between two objects that allows them to be seen as separate and distance. There are two procedures that can be used to evaluate the spatial resolution capabilities of a CT scanner. In the first method an edge is measured to determine the point spread function (PSF). The PSF is then mathematically transformed to obtain the modulation

transfer function (MTF) (47). This process takes considerable time and requires special software. In the second method is simple, faster and is explained in the following procedure.

Measure the MTF by means of the modulation M method (48)**.**

Theory

Coltman has shown that the MTF can be derived from image of cyclic bar pattern (49). His method relies upon the measurement of output amplitude *A(f)* for a square-wave input amplitude A_O of f cycles per unit distance. The MTF is determined according to the formula

$$MTF(f) = \frac{\pi}{4A_0} \times \left(A(f) + \frac{A(3f)}{3} - \frac{A(5f)}{5} + \frac{A(7f)}{7} \cdots \right) \quad (9)$$

A square wave of frequency *f* can be considered to be a sum of sinusoidal components of frequency *f*, *3f*, *5f*, etc. If the MTF is zero at the cutoff frequency *fc* and greater, the square-wave amplitudes will be zero at such frequencies. Therefore, Coltman's formula simplifies to

$$MTF(f) = \frac{\pi A(f)}{4A_0}, \quad f \geq fc/3 \quad (10)$$

For these frequencies, a square-wave input will result in a sinusoidal output because no higher-order terms of the sinusoidal series will be reproduced in the image. This fact enables one to utilize the relationship that exists between signal amplitude and its variance M^2. For the square-wave input, $M^2_O = A^2_O$. For the sinusoidal output, $M^2 = 1/2A^2$. Substituting for these relationships, Equation (10) becomes

$$MTF(f) = \frac{\pi\sqrt{2}}{4} \cdot \frac{M(f)}{M_0}, \quad f \geq fc/3 \quad (11)$$

This relationship is more practical to apply in the case of CT scanners. In the presence of CT noise, the image amplitude *A(f)* is difficult to determine. However, the standard deviation *M(f)* is easily measured. The CT manufacturer typically supplies software to enable to mean and standard deviation to be measured within a region of interest (ROI) in the image. In the presence of noise, this measured value *M'* can be corrected for the effect of noise by the relationship

$$M(f) = \sqrt{M'^2 - N^2}, \tag{12}$$

where N is the standard deviation of the CT image values within a "uniform" ROI (50). To calculate M_O, the formula

$$M_0 = \left|CT_1 - CT_2\right| \sqrt{\frac{n_1 \cdot n_2}{n^2}} \tag{13}$$

is used (50). Here n_1 is the number of pixels of value CT_1 in the object, n_2 is the number of pixels of value CT_2, and $n = n_1 + n_2$. This simplifies to

$$M_0 = \frac{\left|CT_1 - CT_2\right|}{2}, \tag{14}$$

when the ROI contains many pixels and $n_1 = n_2$.

The value $M'(f)$ was measured for each pattern within the array using the largest possible square ROI which could be contained within the boundaries of the pattern. M_O (Equation 14) was determined by a measurement of the CT value of Plexiglass (CT_p) at the location shown in Figure 11, and a measurement of the CT value of water (CT_w) at the same (x, y) coordinate when the phantom was incremented to image a "water only" slice. The standard deviations N_p and N_w were also determined at these locations to derive an estimate of noise $N^2 = (N^2_p + N^2_w)/2$. The measured M' values were corrected for noise (Equation 12), then used to compute MTF(f) points (Equation 11).

Figure 11 is an example of a CT image (technique; head 160 mA, 25 cm SFOV, 1.25 mm 4i slice thickness) of the bar pattern phantom with window width and level adjusted to improve contrast between water and plexiglass. The ROIs are used for calculating mean water and plexiglass pixel values and the standard deviation of a bar pattern. Only the four bar patterns at spatial frequencies of 3.1, 3.8, 5.0 and 6.3 line pairs per cm are resolved in this image.

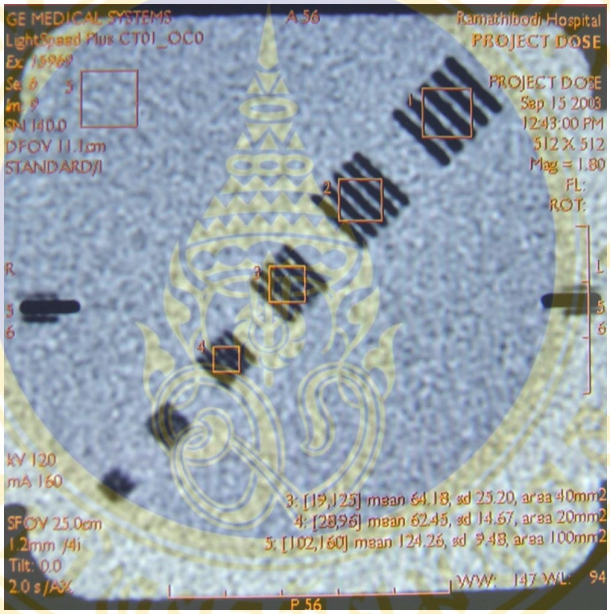

Figure 11. Standard software allows the standard deviation *M'* to be calculated within the bar pattern as shown. In addition, the mean CT_p (124.26) and standard deviation N_p (9.48) for uniform plexiglass can also be determined. The MTF values are calculated from this data as shown in Table 5. (An additional image of a "water only" slice was used to obtain CT_w = -2.89 and N_w = 7.95 HU).

Table 5. *M'* values (Figure 11) are corrected for noise $N = 9.48$ to derive M values. The MTF values are calculated by Equation 11, as the following example.

Bar size (mm)	1.6	1.3	1.0	0.8
M'(HU)	42.87	34.70	25.20	14.67
$N^2 = (N_p^2 + N_w^2) / 2$	$= (9.48^2 + 7.95^2) / 2 = 76.536$			
$M(f) = \sqrt{M'^2 - N^2}$ *(HU)*	41.97	33.58	23.63	11.78
$M_o = (CT_p - CT_w) / 2$	$= (124.26 - (-2.89)) / 2 = 63.575$			
$MTF(f) = \frac{\pi\sqrt{2}}{4} \cdot \frac{M(f)}{M_0}$	0.7332	0.5867	0.4129	0.2057
MTF at *f* cycles/cm	73.32 % at 3.1	58.67 % at 3.8	41.29 % at 5.0	20.57 % at 6.3

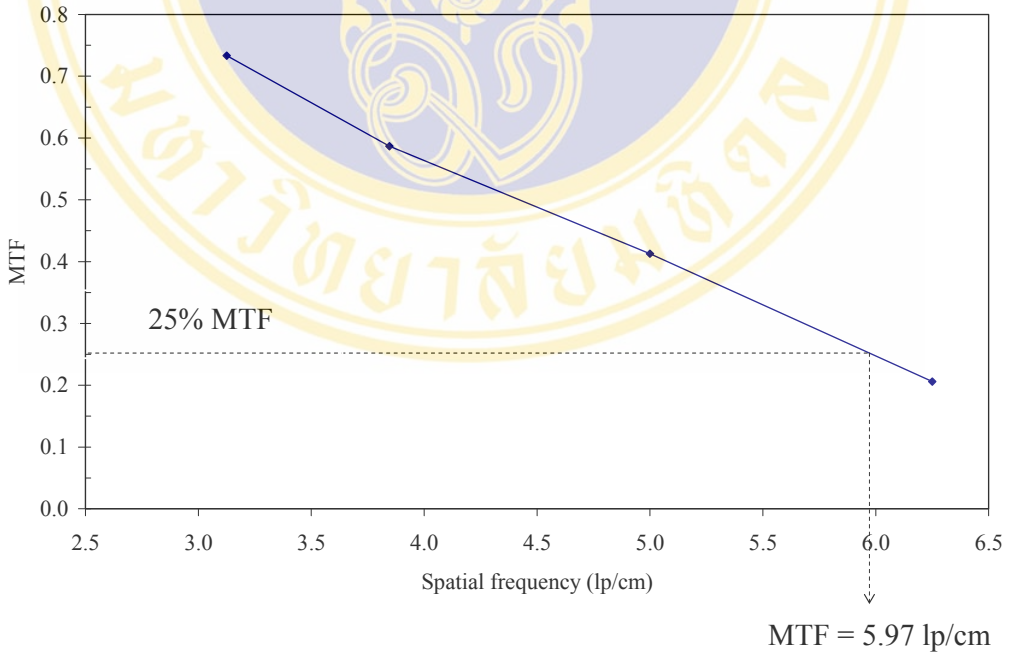

Figure 12. Graph of the %MTF versus the spatial frequency of bar pattern (lp/cm).

4.2.5.2 Low contrast resolution

Low contrast resolution refers to the capability of the CT system to distinguish relatively large objects which differ only slightly in density from background or demonstrate subtle differences in tissue densities from one region of anatomy to another. Typically, contrast resolution is expressed in one of two ways: the smallest diameter of an object with a specific contrast that can be detected or smallest difference in x-ray attenuation that can be discriminated for object of a specific diameter (47).

In this study, a score of low contrast detectability (51) was calculated by the following method. The visualization of each object in each row was graded on a four level scale as shown in Figure 13. Grade 2.0 was assigned when the object was visible and appeared as a perfect circle, grade 1.5 was assigned when the object was appeared like a circle, grade 1.0 was assigned when the object was not a circle but the object size was bigger than 50%, grade 0.5 was assigned when the object size was smaller than 50%.

The low contrast score obtained by adding the grade values for each object (5 holes in 1 row) in each row (9 holes size). And in this study were considered only the objects in 7 holes size.

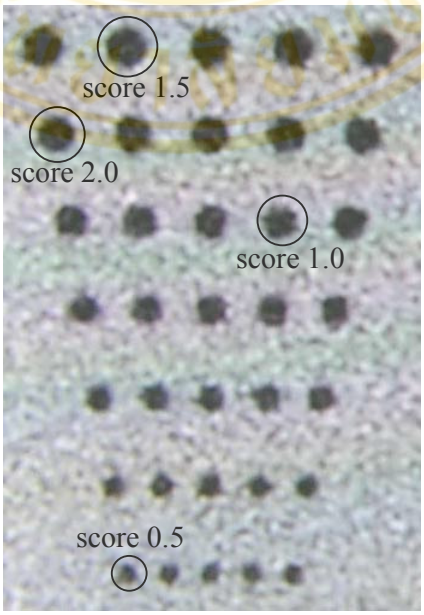

Figure 13. CT image of the low contrast detection phantom.

4.2.5.3 Image noise

Ideally, a CT scan of a uniform phantom would have uniform pixel values (CT numbers) throughout the phantom image. In reality, the CT numbers in an image of homogeneous phantom are not uniform. The variation in pixel intensities has random and systemic components. The random component of image nonuniformity is noise. Noise influences mainly the possibility to detect the details at low contrast, when the object tends to fade into fluctuations of the signal.

The most common measure of noise is the standard deviation of pixel values in a region of interest (ROI) within a uniform phantom in Hounsfield units (HU) (47).

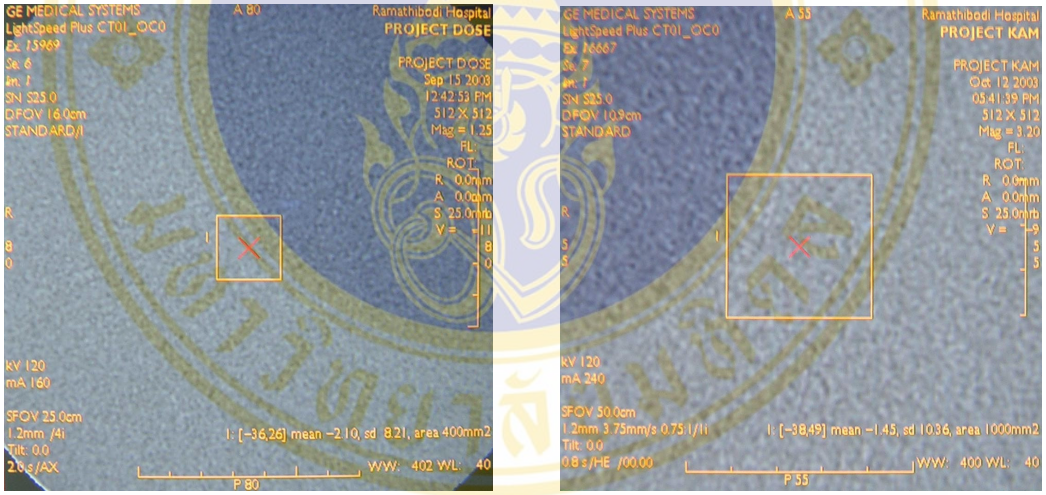

a. b.

Figure 14. Water phantom images: (a) 400 mm^2 ROI for noise measurement of head protocols, (b) 1000 mm^2 ROI for noise measurement of body protocols.

4.2.6 Dose calculation (44)

The dose length product serves as a measure for the dose integral across a dose profile created by a CT unit. The product of dose and length of the irradiated chamber volume is displayed. The result of a measurement in air kerma length product is

$$k_a \cdot 1 = k_Q \cdot k_D \cdot N_a \cdot M \quad (15)$$

where k_a is the air kerma length product in mGy.cm, M is the uncorrected display reading (in Gy.cm) and N_a the calibration factor of the ionization chamber (N_a = 1.00 N_a' = 14,740 Gy.cm/C; Calibration certificate No. 032830). k_D and k_Q are factor to correct for deviations from the reference conditions during the calibration.

Air density correction (k_D)

The correction factor for air density is calculated according to the following formula:

$$k_D = \frac{p_O \cdot (t + 273)}{p \cdot T_O} \quad (16)$$

in this formula t is the temperature in ^{o}C and p the absolute air pressure in hPa at the measuring point. The reference values T_o and p_o are:

T_o = 293 K (20 ^{o}C)

p_o = 1013.2 hPa

The reference value has to be adjusted according to the test certificate delivered with the ionization chamber.

Correction for radiation quality (k_Q)

The calibration factor refers to a distinct radiation quality. If another radiation quality is used, a correction factor k_Q has to be applied. As a standard, each ionization chamber is initially set to k_Q = 1.

CHAPTER V
RESULTS

5.1 Image analysis

CT images acquired with variations from the standard protocols which divided into two scan parts: head (routine head) and body (upper abdomen) were evaluated for image quality. Image quality was evaluated in terms of spatial resolution (25% MTF), low contrast resolution (low contrast scores) and image noise (SD).

5.1.1 Spatial resolution

Modulation transfer function at 25% (25% MTF) was used as an indicator for systemic spatial resolution in this study. When varying scanning parameters as described in previous section, there were minimal differences in spatial resolution observed. The ranges of 25% MTF of all protocols were 5.68 - 6.40 lp/cm in head protocols and 5.48 - 7.17 lp/cm in body protocols.

Table 6, 7 show the spatial resolution of all head and body protocols, respectively. In both protocols, there were some of peak value of 25% MTF, such as 6.40 (105 mA 1.25 slice thickness), 6.32 (100 mA 1.25 slice thickness), 6.30 (130 mA 1.25 slice thickness), 6.29 (155 mA 1.25 slice thickness) and 6.27 (130 mA 1.25 slice thickness) in head protocols, 7.17 (140 mA, 1.25 mm slice thickness), 6.73 (140 mA, 1.25 mm slice thickness) and 6.61 (160 mA, 2.5 mm slice thickness) in body protocols.

Figure 15, 16 show the spatial resolution of maximum and minimum setting in each scanning parameters. In head protocols (Figure 15) there are 160 and 100 mA, 10 and 1.25 mm in slice thickness, 0.98 and 0.49 mm pixel size. In body protocols (Figure 16) there are 240 and 140 mA, 10 and 1.25 mm in slice thickness, 0.98 and 0.49 mm pixel size, 1.5 and 0.75 in pitch.

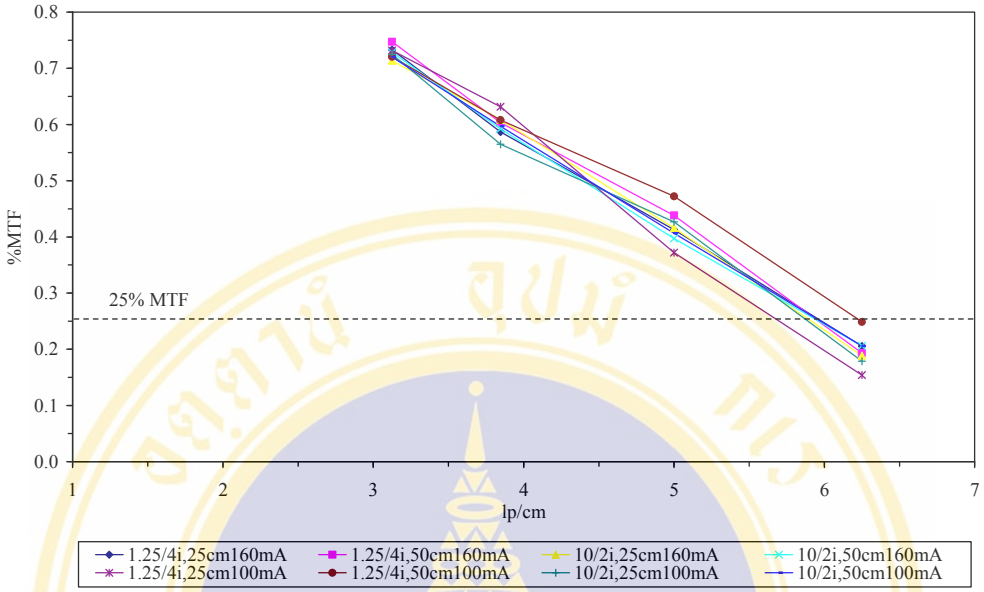

Figure 15. Graph of spatial resolution at 25% MTF with various scan parameter in head scanning. For the sequences that follow above graph the 25% MTF are 5.97, 5.97, 5.93, 5.93, 5.72, 6.32, 5.87 and 5.97, respectively.

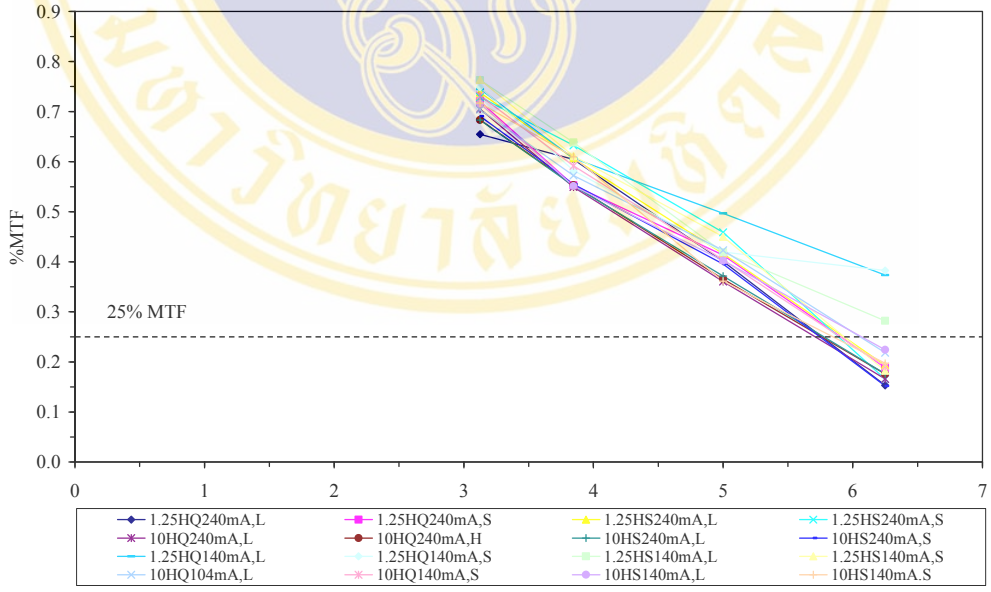

Figure 16. Graph of spatial resolution at 25% MTF with various scan parameter in body scanning. For the sequences that follow above graph the 25% MTF are 5.76, 5.88, 5.93, 5.91, 5.70, 5.76, 5.77, 5.72, 7.17, 6.73, 6.29, 5.94, 6.06, 5.89, 6.00 and 5.83, respectively.

5.1.2 Low contrast resolution

Table 8, 9 show the low contrast resolution for variations of head and body protocols, respectively. Low contrast scores from both head and body protocols were found dependent on the slice thickness. We found that low contrast detectability improved when slice thickness setting was increased, as some selected examples from head scanning protocols in Figure 17.

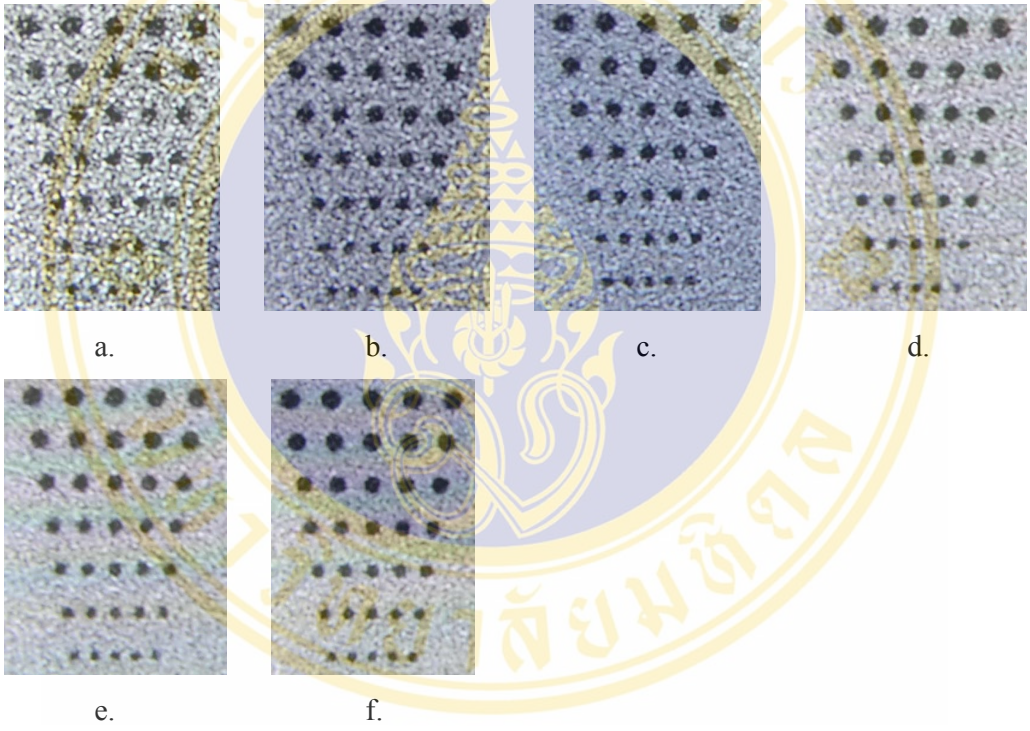

Figure 17. Low contrast phantom images of head with various slice thickness, constant mA (160) and SFOV (25 cm). (a) 1.25 mm/4i low contrast score 28.5, (b) 2.5 mm/2i low contrast score 28.5, (c) 3.75 mm/4i low contrast score 32.5, (d) 5 mm/1i low contrast score 35, (e) 7.5 mm/2i low contrast score 34.5, (f) 10 mm/1i low contrast score 39.

In both head and body protocols, low contrast scores were found dependent on tube current. Low contrast scores were decreased as the tube current decreased. The pixel size selection did not affect low contrast score in all examination protocols.

For routine body scanning protocols, helical mode is normally selected. This study showed that low contrast score was slightly dependent on pitch. In thick slice thickness (7.5 and 10.0 mm), low contrast score increased as pitch decreased, however, in thin slice thickness (1.25, 2.5, 3.75 and 5.0 mm) pitch selection did not affect low contrast score. Figure 18 shows dependence of low contrast scores with the pitch selection in the body scanning protocols.

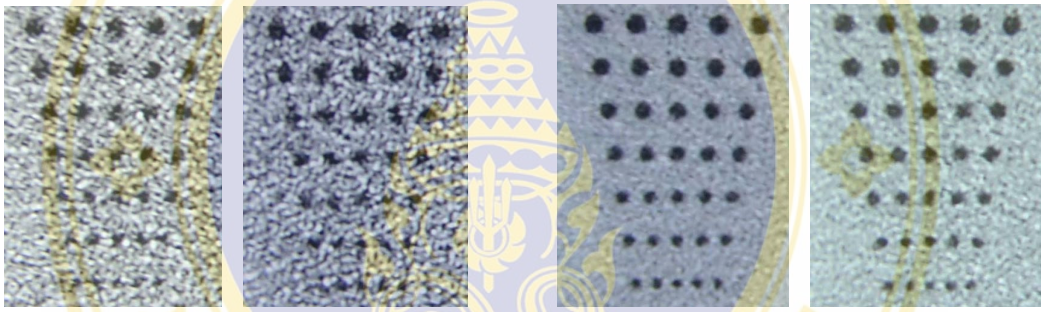

a. b. c. d.

Figure 18. Low contrast phantom images of body with various pitch, constant mA (240), SFOV (50 cm). (a) 26.5 low contrast score of pitch 0.75 slice thickness 1.25 mm, (b) 26 low contrast score of pitch 1.5 slice thickness 1.25 mm, (c) 38 low contrast score of pitch 0.75 slice thickness 10 mm, (d) 30.5 low contrast score of pitch 1.5 slice thickness 10 mm.

5.1.3 Image noise (SD)

Table 10, 11 show the image noise (standard deviation; SD) for variation of head and body protocols, respectively. Image noise from both head and body protocols were inversely dependent on slice thickness and tube current which SD decreased as these two parameters were increased, as some selected examples shown in Figure 19 and 20. On the other hand SD was directly dependent on pixel size and pitch, where SD increased with increasing pixel size and pitch.

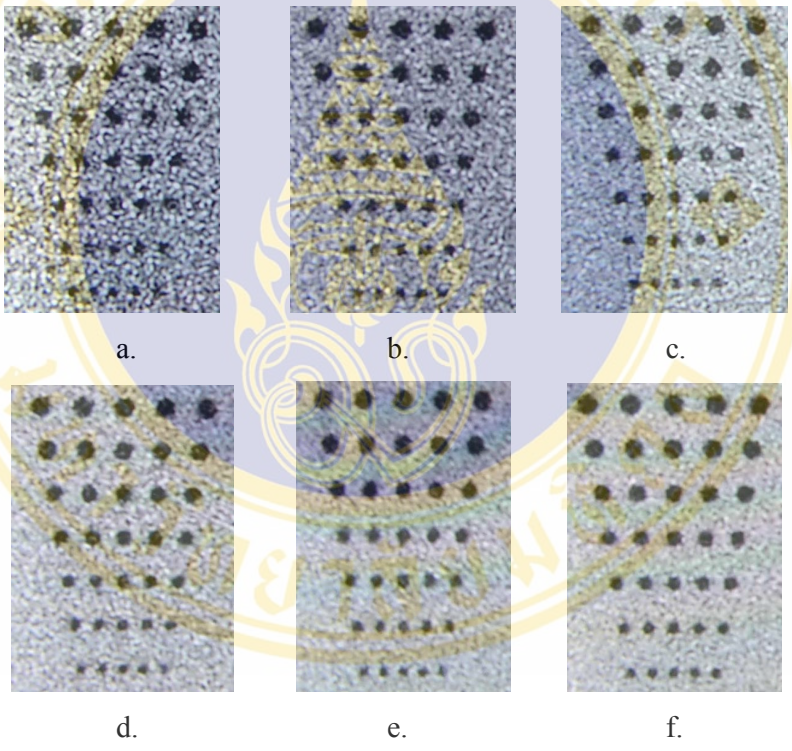

Figure 19. Phantom images of head with various slice thickness, constant mA (160), SFOV (25 cm). (a) 1.25 mm/4i SD 8.21, (b) 2.5 mm/2i SD 5.86, (c) 3.75 mm/4i SD 4.30, (d) 5 mm/1i SD 3.68, (e) 7.5 mm/2i SD 3.24, (f) 10 mm/1i SD 2.71.

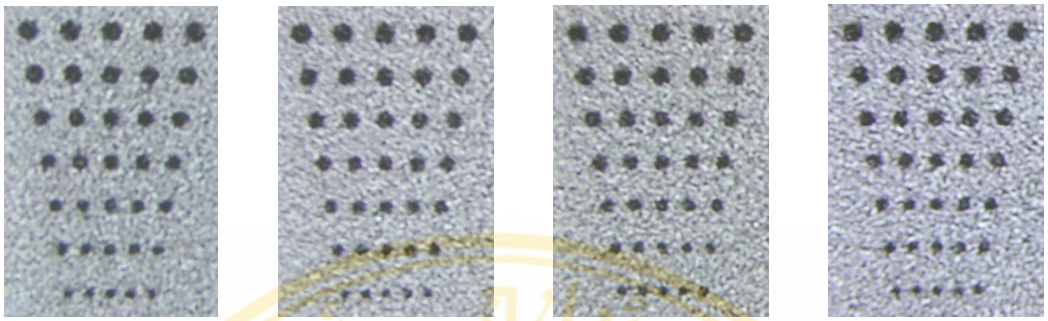

a. b. c. d.

Figure 20. Phantom images of head with various mA, constant slice thickness (5.0 mm/1i), SFOV (50 cm). (a) 160 mA SD 4.27, (b) 140 mA SD 4.41, (c) 120 mA SD 4.58, (d) 100 mA SD 5.61.

5.2 Dose measurement

The DLP_{air} data which divided into four scan sections; head axial posterior fossa, head axial above posterior fossa, body helical pre-contrast and body helical post-contrast are provided in Table 12, 13 and 14, respectively. For Figure 21, 22 and 23 show the correlation between DLP_{air} and various scan parameters.

In both head and body protocols, DLP_{air} were found increased linearly with increasing tube current. In multi-detector CT, slice thickness (data in Table 12-14) is not a factor to investigate radiation dose characteristics because it dose not correspond to the total nominal scan width (T'). Instead, total nominal scan width is determined by the x-ray beam collimation, is the factor affecting the dose.

In axial CT (Table 15, 16), two parameters affecting dose were the CT mode (1i, 2i or 4i modes) and the desired slice thickness. In helical CT (Table 17-20), these parameters were the mode (high quality or high speed) and the table speed. This study demonstrated that axial and helical dose values tend to decrease when the total nominal scan width increases.

In helical mode, a change in the slice thickness did not change the radiation dose. For example, in high speed of 15 mm per rotation, the total nominal scan width is 10 mm; with body-post contrast, 240 mA and 50 cm SFOV the DLP_{air} are 226.55,

229.94 and 234.37 mGy.cm for 2.5 mm, 3.75 mm and 5.0 mm reconstructed slices, respectively.

Similar a result in axial mode with head posterior fossa protocol and 5 mm nominal x-ray beam width. However, this result was not found in head above posterior fossa protocol which the radiation dose were at least (under 32 mGy.cm).

In all protocols, DLP_{air} was higher in smaller pixel sizes. Dose differences when compare between each one scan protocol in 4 subdivide parts of the examination: head posterior fossa, head above posterior fossa, body pre-contrast and body-post contrast are 16.97-17.88 %, 11.36-16.58 %, 16.38-17.29 % and 16.11-17.61 %, respectively.

In body helical, DLP_{air} was increased when decreased pitch. When comparison made between two pitch, DLP_{air} of lower pitch (pitch = 0.75) was double to the other higher pitch (pitch = 1.5).

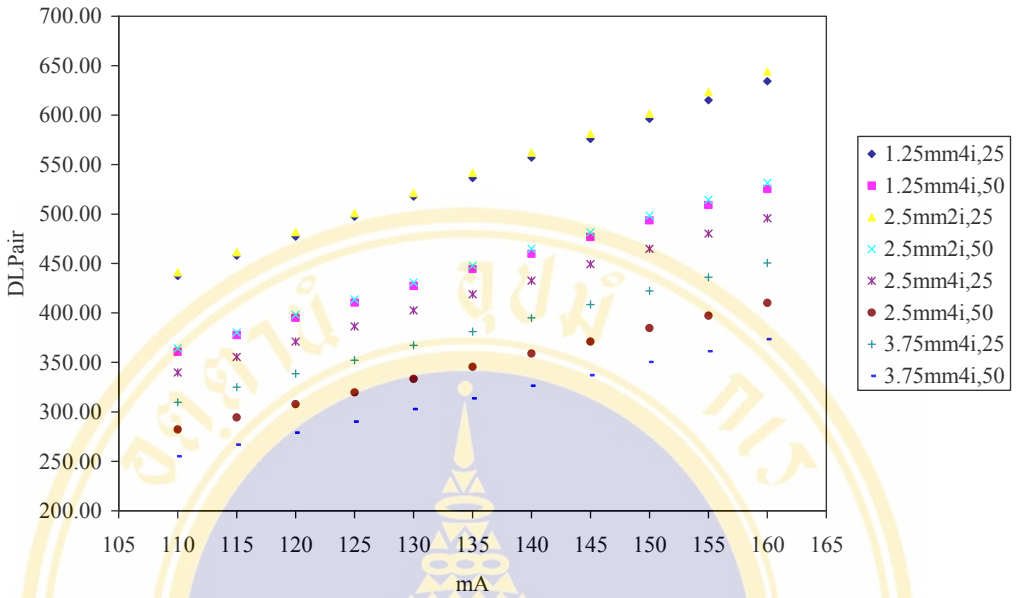

a.

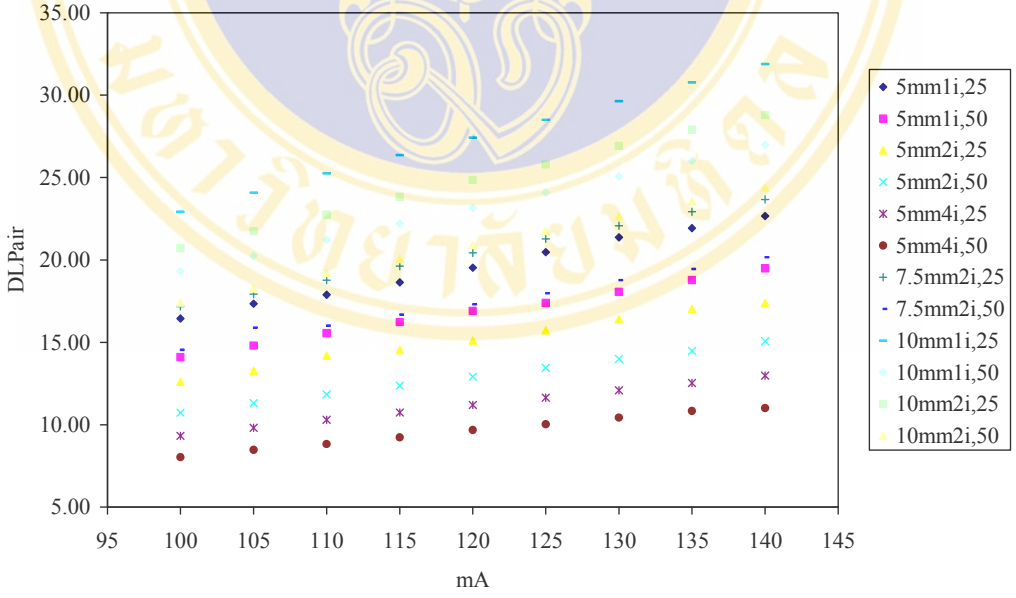

b.

Figure 21. DLP_{air} as a function of scan parameters: mA, slice thickness and pixel size in head protocols (a) posterior fossa, (b) above posterior fossa.

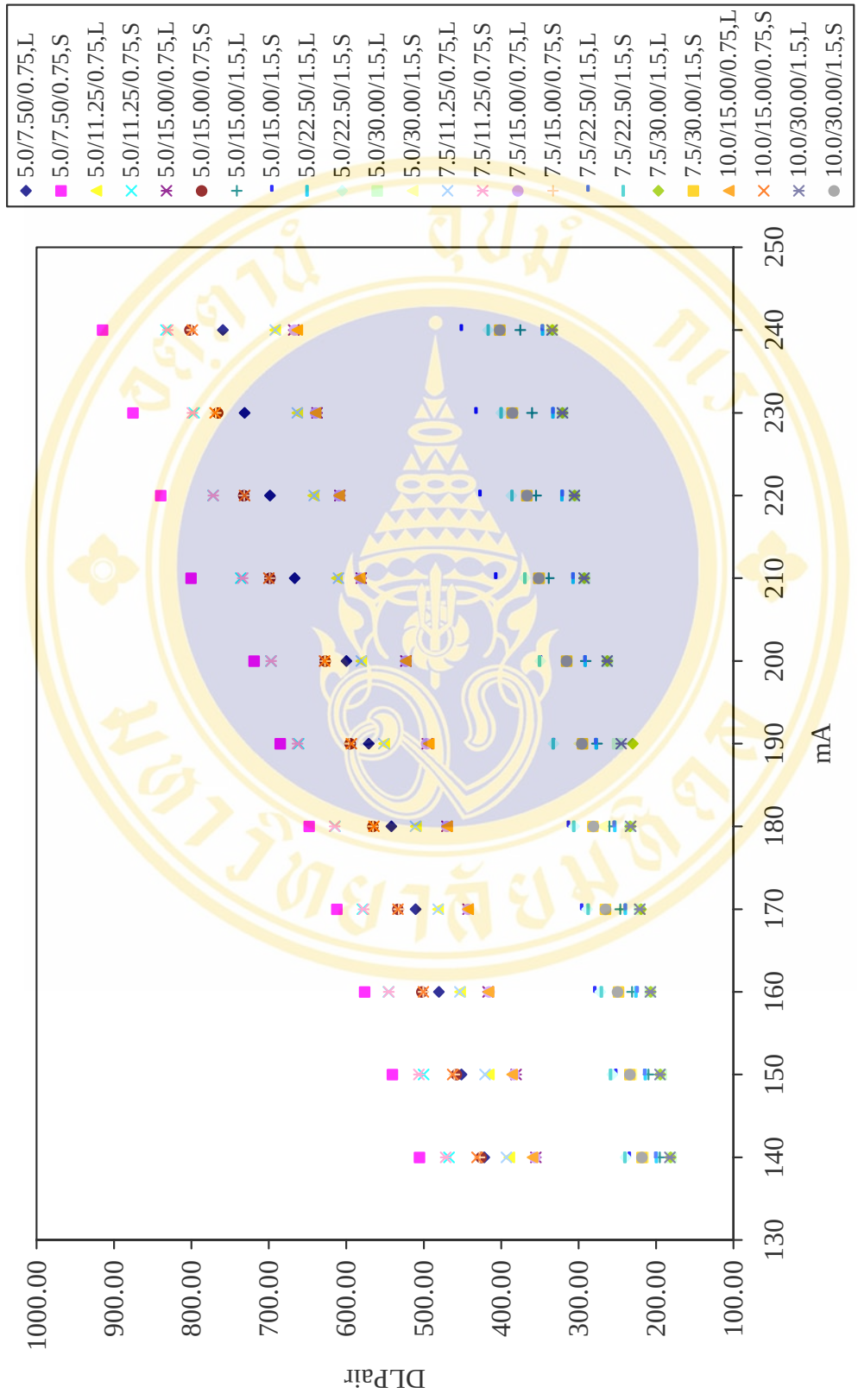

Figure 22. DLP_{air} as a function of scan parameters; mA, slice thickness, pixel size and pitch in body pre contrast.

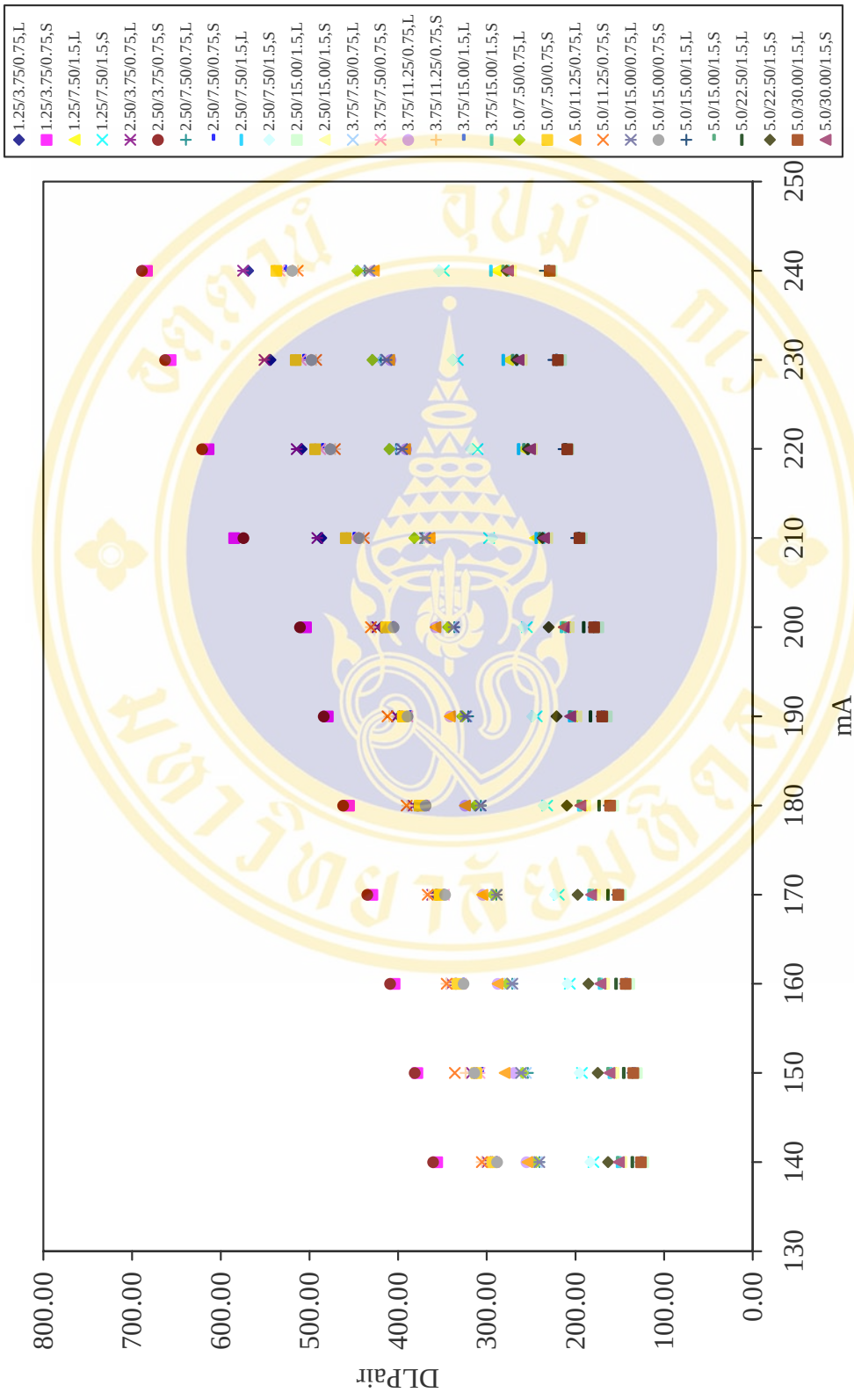

Figure 23. DLP_{air} as a function of scan parameters; mA, slice thickness, pixel size and pitch in body post contrast.

Table 6. Varied parameters and 25% MTF (lp/cm) of head.

Thickness	SFOV (cm)	mA												
		160	155	150	145	140	135	130	125	120	115	110	105	100
1.25mm/4i	25	5.97	6.29	6.17	6.11	5.97	5.92	6.30	6.10	6.00	5.86	5.91	6.09	5.72
	50	5.97	6.20	6.01	6.09	6.15	6.02	6.27	5.96	5.93	5.81	6.22	6.40	6.32
2.50mm/2i	25	6.06	5.92	5.94	5.91	5.90	6.05	5.89	5.74	5.86	5.81	6.04	6.14	6.14
	50	5.81	6.08	5.86	6.11	6.05	6.05	6.16	6.23	5.98	5.89	5.98	5.90	6.00
2.50mm/4i	25	5.99	5.96	6.05	5.93	6.00	5.91	6.07	6.10	5.88	5.68	6.13	6.04	5.94
	50	5.99	5.76	5.94	5.82	6.14	5.95	5.91	5.80	6.21	5.96	6.02	5.89	5.95
3.75mm/4i	25	5.96	5.86	6.03	6.11	5.91	5.99	5.91	5.84	5.92	5.87	5.88	5.86	5.93
	50	5.95	6.05	5.84	5.88	5.91	5.84	5.88	5.97	5.95	5.88	5.80	6.00	5.91
5.00mm/1i	25	5.93	5.87	6.03	5.90	5.97	5.89	5.95	5.99	6.00	5.99	5.86	5.82	5.89
	50	6.02	6.05	5.93	5.93	5.97	6.05	6.04	5.95	5.93	6.00	6.18	6.04	6.13
5.00mm/2i	25	6.00	5.89	5.97	5.93	6.09	5.89	5.83	6.04	5.94	5.88	6.08	5.83	5.99
	50	5.95	5.98	5.86	6.00	5.97	6.06	5.99	5.94	5.93	6.04	5.92	5.87	6.12
5.00mm/4i	25	5.90	6.04	5.95	6.11	6.04	5.90	5.91	5.98	5.88	5.88	6.10	5.90	5.93
	50	5.96	5.97	6.08	5.97	5.96	5.95	5.99	5.93	5.93	5.82	5.82	5.95	5.77
7.50mm/2i	25	5.92	5.87	5.92	6.04	6.09	5.93	6.02	5.95	6.00	5.91	5.87	5.83	5.96
	50	5.86	5.96	5.91	5.89	5.92	5.84	6.01	5.91	5.95	5.80	6.01	5.91	5.92
10.0mm/1i	25	5.96	5.94	5.89	5.92	5.86	5.96	5.90	5.91	5.98	5.92	5.92	5.91	5.95
	50	5.94	5.94	6.03	5.93	5.97	5.94	5.89	5.91	5.96	5.97	5.93	5.91	6.01
10.0mm/2i	25	5.93	5.88	5.88	5.84	5.89	5.96	5.99	5.92	5.92	5.83	5.93	5.94	5.87
	50	5.94	5.95	5.91	5.87	5.94	5.90	5.90	5.87	5.91	5.95	5.86	5.91	5.97

Table 7. Varied parameters and 25% MTF (lp/cm) of body.

Thickness/ Speed/Pitch	SFOV/DFOV (cm)	mA										
		240	230	220	210	200	190	180	170	160	150	140
1.25/3.75/0.75	50/35	5.76	5.73	5.85	6.13	5.83	5.80	6.04	6.29	6.28	5.73	7.17
	25/25	5.88	5.93	6.08	5.62	6.28	5.99	6.25	5.89	6.35	5.81	6.73
1.25/7.50/1.5	50/35	5.93	5.58	6.07	5.59	6.04	6.21	6.28	5.58	6.26	5.70	6.29
	25/25	5.91	5.94	6.19	5.95	6.39	6.49	5.87	6.32	6.25	5.77	5.94
2.50/3.75/0.75	50/35	6.15	5.83	5.70	5.81	6.12	6.41	6.09	6.11	6.20	5.93	6.34
	25/25	5.82	5.61	5.74	5.74	5.97	5.88	6.30	6.21	6.16	6.06	6.22
2.50/7.50/0.75	50/35	5.80	5.91	5.94	5.77	6.23	6.17	6.05	6.20	5.91	5.98	6.22
	25/25	5.76	5.68	5.86	6.00	6.04	6.15	5.86	5.89	5.82	5.91	6.11
2.50/7.50/1.5	50/35	6.32	6.11	6.04	5.48	6.29	5.91	6.07	6.04	5.88	6.39	6.05
	25/25	5.79	5.87	5.69	5.81	6.24	6.28	6.11	6.28	6.23	6.11	6.11
2.50/15.00/1.5	50/35	5.73	5.70	5.86	6.07	6.13	6.36	6.10	6.14	6.61	5.92	5.81
	25/25	6.00	5.93	5.77	5.82	6.45	5.89	6.07	6.40	5.94	5.87	6.08
3.75/7.50/0.75	50/35	5.85	5.86	5.85	5.81	6.02	6.03	5.86	6.18	5.80	5.99	6.03
	25/25	5.70	5.98	5.82	5.70	5.88	5.88	5.99	5.87	6.22	6.06	6.00
3.75/11.25/0.75	50/35	5.89	5.91	5.80	5.57	6.03	6.03	5.98	6.10	6.04	6.23	5.96
	25/25	5.82	5.88	5.90	5.53	5.93	6.10	6.03	5.89	5.99	5.87	5.91
3.75/15.00/1.5	50/35	5.71	6.02	5.90	6.07	5.94	5.95	6.07	5.86	6.15	6.14	5.99
	25/25	5.82	5.98	5.78	5.76	5.96	6.01	5.99	6.26	6.06	6.20	6.03
5.0/7.50/0.75	50/35	5.90	5.87	5.84	5.84	6.15	6.16	6.17	6.06	6.06	5.97	6.01
	25/25	5.79	5.80	5.83	5.85	5.92	6.01	6.01	5.98	6.02	6.06	6.12
5.0/11.25/0.75	50/35	5.84	5.72	5.72	6.11	6.04	5.91	6.00	5.93	5.99	5.91	5.93
	25/25	5.84	5.87	5.80	6.00	5.91	5.91	6.11	6.09	5.94	6.05	5.93
5.0/15.00/0.75	50/35	5.93	5.88	5.65	5.80	5.98	5.96	6.02	5.83	6.14	5.84	5.87
	25/25	5.78	5.88	5.70	5.66	5.97	5.80	5.84	5.96	6.06	6.01	5.95
5.0/15.00/1.5	50/35	5.69	5.77	5.81	6.11	5.96	6.20	6.13	6.07	6.24	5.97	5.77
	25/25	5.94	5.75	5.89	5.95	5.99	5.86	6.10	6.18	6.08	5.92	6.29
5.0/22.50/1.5	50/35	5.75	5.73	5.86	6.06	5.96	6.07	5.97	6.00	6.10	5.80	6.02
	25/25	5.81	5.83	5.94	5.88	5.94	6.07	6.07	6.06	6.12	6.22	6.04
5.0/30.00/1.5	50/35	5.84	5.71	5.81	5.81	5.83	5.99	5.95	6.23	5.84	5.86	5.97
	25/25	5.98	5.81	5.95	5.81	6.01	6.28	5.85	6.42	6.03	6.03	6.13
7.5/11.25/0.75	50/35	5.68	5.70	5.88	5.80	5.96	5.98	5.98	5.97	5.84	5.80	6.07
	25/25	5.93	5.97	5.80	5.83	5.95	6.01	5.89	5.99	5.85	5.86	5.83
7.5/15.00/0.75	50/35	5.83	5.75	5.76	5.81	5.84	5.98	6.01	5.92	5.90	5.90	5.87
	25/25	5.74	5.78	5.84	5.85	6.01	6.06	5.93	5.95	5.89	5.95	5.83
7.5/22.50/1.5	50/35	5.79	5.70	5.80	5.70	5.95	6.04	5.90	6.01	5.94	5.90	5.81
	25/25	5.88	5.88	5.65	5.96	6.22	6.01	5.99	5.99	6.18	5.86	6.05
7.5/30.00/1.5	50/35	5.80	5.89	5.85	5.82	5.96	5.95	6.05	5.81	5.93	5.85	5.85
	25/25	5.65	5.96	5.84	5.83	6.10	5.97	6.01	6.05	6.07	6.03	5.80

Table 7. Varied parameters and 25% MTF (lp/cm) of body. (Continued)

Thickness/ Speed/Pitch	SFOV/DFOV (cm)	mA										
		240	230	220	210	200	190	180	170	160	150	140
10.0/15.00/0.75	50/35	5.70	5.69	5.71	5.78	6.06	5.94	5.97	5.89	5.89	5.89	6.06
	25/25	5.76	5.78	5.79	5.72	5.93	5.93	5.89	5.92	6.02	5.92	5.89
10.0/30.00/1.5	50/35	5.77	5.75	5.91	5.76	5.86	6.04	5.95	6.05	5.95	6.06	6.00
	25/25	5.72	5.86	5.76	5.79	5.94	6.05	5.99	5.91	5.93	6.08	5.83

Table 8. Varied parameters and low contrast score of head.

Thickness	SFOV (cm)	mA												
		160	155	150	145	140	135	130	125	120	115	110	105	100
1.25mm/4i	25	28.5	28.0	25.5	25.5	24.5	26.0	25.0	26.5	28.0	25.5	27.5	25.5	25.0
	50	26.5	28.5	26.0	27.0	27.0	24.5	28.5	29.5	26.5	27.0	28.0	24.5	26.0
2.50mm/2i	25	28.5	30.5	29.0	30.0	29.0	31.5	32.0	31.5	30.0	31.5	32.5	31.0	30.0
	50	30.0	28.0	29.5	29.5	28.0	30.5	32.5	31.5	31.0	31.5	32.5	29.5	27.5
2.50mm/4i	25	30.0	33.0	29.5	32.0	28.5	30.5	29.0	30.5	34.0	32.0	32.5	32.0	26.5
	50	29.5	28.5	31.5	30.0	29.5	31.0	30.5	32.5	30.0	31.0	33.0	32.0	30.0
3.75mm/4i	25	32.5	31.0	30.5	31.5	34.5	32.0	31.0	33.0	33.0	32.0	34.0	32.5	30.0
	50	33.0	31.0	31.5	31.5	33.0	32.0	30.0	31.0	33.5	32.0	34.5	34.0	27.5
5.00mm/1i	25	35.0	33.0	32.5	37.0	33.5	31.5	32.5	33.0	34.5	34.5	35.5	35.5	32.5
	50	33.0	32.5	33.0	33.5	33.5	34.0	33.5	34.0	34.5	34.0	35.0	33.0	31.5
5.00mm/2i	25	33.5	32.5	34.0	33.0	33.0	34.5	33.0	34.5	35.5	32.5	34.0	32.0	31.5
	50	34.5	33.0	34.0	34.0	35.0	34.5	34.0	33.0	35.5	34.0	34.5	33.5	32.5
5.00mm/4i	25	35.5	32.5	34.0	33.0	33.0	32.5	36.0	32.0	33.5	31.5	35.0	33.5	30.0
	50	33.0	32.5	35.5	34.0	32.0	34.5	34.0	34.0	32.5	33.5	33.5	32.5	30.5
7.50mm/2i	25	34.5	33.5	35.0	34.5	35.0	35.0	35.5	36.5	35.5	35.0	36.0	34.0	34.0
	50	37.5	35.0	34.0	34.0	35.0	35.0	38.5	36.5	34.0	36.5	36.5	35.5	34.5
10.0mm/1i	25	39.0	35.5	37.5	37.5	36.0	33.5	39.0	36.5	36.5	36.0	35.0	35.5	35.0
	50	38.5	37.0	39.5	36.0	36.5	33.5	35.0	37.0	38.5	35.5	37.0	35.0	35.0
10.0mm/2i	25	38.0	38.0	37.5	36.5	35.5	36.0	37.5	36.5	38.5	37.0	34.0	36.0	35.5
	50	36.0	36.5	38.0	35.5	35.0	34.5	36.0	36.0	37.0	36.0	37.5	35.0	35.5

Table 9. Varied parameters and low contrast score of body.

Thickness/ Speed/Pitch	SFOV/DFOV (cm)	mA										
		240	230	220	210	200	190	180	170	160	150	140
1.25/3.75/0.75	50/35	26.5	23.5	23.5	24.5	24.0	20.5	23.5	22.5	21.0	21.5	22.0
	25/25	25.5	24.0	23.0	23.5	22.0	21.5	25.0	22.0	20.5	18.5	23.5
1.25/7.50/1.5	50/35	26.0	22.0	21.5	20.5	21.5	20.0	23.5	21.0	19.0	20.0	23.0
	25/25	25.5	24.0	21.5	21.5	21.0	20.5	23.5	19.5	18.5	19.5	18.0
2.50/3.75/0.75	50/35	28.5	28.5	26.0	27.0	26.0	25.5	26.0	25.0	24.5	22.0	27.5
	25/25	29.5	30.0	24.5	28.5	25.0	25.0	27.5	26.0	26.0	24.5	25.5
2.50/7.50/0.75	50/35	30.5	26.0	27.5	25.0	25.5	26.0	26.5	23.5	24.0	22.5	24.0
	25/25	27.0	25.0	27.0	24.5	26.0	25.5	27.0	21.0	23.5	23.5	21.0
2.50/7.50/1.5	50/35	26.0	24.5	24.0	23.5	23.0	21.5	23.5	23.5	21.5	23.0	21.0
	25/25	25.5	24.5	23.5	22.5	24.5	22.0	20.0	22.5	22.0	20.0	22.0
2.50/15.00/1.5	50/35	27.5	26.0	26.0	28.0	25.5	23.5	23.0	23.0	23.0	22.0	23.5
	25/25	27.5	27.5	24.5	25.5	22.5	22.5	23.5	22.0	20.5	18.5	23.0
3.75/7.50/0.75	50/35	29.0	33.0	28.5	29.0	29.5	25.0	28.0	28.5	30.0	24.5	26.0
	25/25	27.5	31.5	27.5	29.5	30.0	28.5	27.0	28.0	29.0	27.0	28.0
3.75/11.25/0.75	50/35	29.5	29.0	27.5	28.0	28.5	24.5	26.0	25.5	27.5	26.0	27.0
	25/25	29.0	28.5	26.5	27.5	26.5	26.5	30.0	27.5	27.0	24.5	25.5
3.75/15.00/1.5	50/35	27.0	25.5	26.5	28.0	27.0	24.0	24.0	26.0	28.5	24.0	23.5
	25/25	29.5	24.5	23.0	25.0	26.5	23.5	28.5	24.0	22.0	22.5	23.0
5.0/7.50/0.75	50/35	30.5	32.0	30.5	28.5	27.5	26.5	25.5	28.5	27.0	29.0	27.5
	25/25	32.5	31.5	28.5	31.0	29.5	26.5	30.0	28.0	28.5	29.5	26.5
5.0/11.25/0.75	50/35	30.0	30.5	27.5	30.0	29.0	29.0	29.5	29.5	27.0	24.0	30.5
	25/25	30.5	32.5	29.5	27.0	30.0	28.0	31.0	27.5	27.5	25.5	29.0
5.0/15.00/0.75	50/35	29.0	28.5	27.5	29.0	27.5	27.0	24.5	29.5	29.0	26.5	29.0
	25/25	34.0	31.0	28.5	29.5	27.5	26.0	26.0	26.5	25.0	24.0	27.0
5.0/15.00/1.5	50/35	30.0	30.0	26.5	27.0	24.5	27.5	25.0	24.5	24.0	24.0	26.5
	25/25	27.5	26.0	29.0	24.0	25.5	26.5	27.0	23.0	25.5	25.0	24.0
5.0/22.50/1.5	50/35	32.0	29.0	27.0	29.0	29.0	26.5	27.0	26.5	27.5	25.5	26.0
	25/25	27.0	26.5	27.5	28.5	30.0	25.0	27.5	29.0	23.5	25.5	24.0
5.0/30.00/1.5	50/35	29.5	28.5	28.5	29.0	27.5	23.5	27.5	26.5	24.5	24.0	25.5
	25/25	28.0	25.5	27.0	30.0	27.5	24.5	27.5	26.0	24.0	27.5	26.5
7.5/11.25/0.75	50/35	36.5	31.0	33.0	32.0	32.0	31.0	31.0	32.0	31.0	31.0	29.0
	25/25	35.0	31.0	31.5	31.0	34.0	31.0	29.5	29.5	30.5	29.5	28.5
7.5/15.00/0.75	50/35	30.0	32.0	34.0	31.5	33.0	31.5	31.0	34.5	27.5	30.0	29.0
	25/25	31.5	34.5	29.0	32.0	31.0	29.0	29.0	32.5	28.5	28.5	29.5
7.5/22.50/1.5	50/35	30.5	29.0	27.5	28.0	30.5	30.5	25.5	28.5	28.0	27.5	27.5
	25/25	28.5	29.5	28.0	28.0	27.5	29.5	26.0	28.5	28.0	28.0	25.5
7.5/30.00/1.5	50/35	32.0	32.0	30.5	28.5	28.0	25.5	28.5	27.5	27.5	27.5	24.5
	25/25	28.5	30.0	28.5	27.5	28.5	26.0	29.0	28.5	26.5	27.0	26.0

Table 9. Varied parameters and low contrast score of body. (Continued)

Thickness/ Speed/Pitch	SFOV/DFOV (cm)	mA										
		240	230	220	210	200	190	180	170	160	150	140
10.0/15.00/0.75	50/35	38.0	34.0	34.5	33.0	32.0	31.0	30.5	31.5	30.5	31.0	31.5
	25/25	35.0	37.0	32.0	30.5	28.5	32.0	30.5	32.0	30.0	32.0	31.5
10.0/30.00/1.5	50/35	30.5	32.0	29.5	29.5	27.5	30.5	29.5	30.5	30.0	28.5	28.5
	25/25	31.0	28.0	30.5	28.5	29.0	28.0	29.0	28.5	27.0	29.0	29.0

Table 10. Varied parameters and standard deviation (SD) of water with ROI area 400 mm^2, head.

Thickness	SFOV (cm)	mA												
		160	155	150	145	140	135	130	125	120	115	110	105	100
1.25mm/4i	25	8.21	8.09	8.33	8.73	8.38	9.24	8.77	8.88	8.82	9.07	9.47	10.50	9.78
	50	8.17	8.62	9.05	9.35	9.24	10.13	9.41	9.76	9.76	10.41	10.39	9.66	11.30
2.50mm/2i	25	5.86	5.69	5.67	5.64	5.78	6.18	5.78	6.75	6.32	6.57	6.76	7.32	6.92
	50	6.33	5.95	6.04	6.59	6.70	6.43	6.38	6.75	6.91	7.09	7.39	7.20	7.23
2.50mm/4i	25	5.73	5.53	5.45	5.91	6.08	5.90	6.02	6.43	6.93	6.59	6.44	6.83	7.02
	50	6.23	6.01	6.48	6.21	6.81	6.22	6.83	6.80	6.86	7.23	7.39	7.95	7.58
3.75mm/4i	25	4.30	4.47	4.75	4.98	4.75	4.98	5.09	5.07	5.12	5.29	5.63	5.46	5.67
	50	4.78	4.97	5.09	5.06	5.02	5.36	5.40	5.37	5.31	5.92	6.32	6.31	6.37
5.00mm/1i	25	3.86	4.21	4.04	4.22	4.45	4.42	4.26	4.39	4.71	4.55	4.76	4.83	4.74
	50	4.27	4.29	4.33	4.22	4.41	4.47	4.58	4.51	4.58	5.05	5.13	5.28	5.61
5.00mm/2i	25	4.09	3.86	3.94	3.84	3.80	4.49	4.14	4.55	4.50	4.66	4.53	5.00	4.87
	50	3.95	4.34	3.94	4.53	4.63	4.85	4.89	4.85	4.90	4.95	4.83	5.27	5.49
5.00mm/4i	25	3.96	3.97	4.13	4.03	4.23	4.31	4.38	4.55	4.56	4.85	5.01	4.73	4.59
	50	4.39	4.27	4.29	4.54	4.48	4.68	4.34	4.68	5.05	4.66	4.88	5.18	5.80
7.50mm/2i	25	3.24	3.04	3.15	3.32	3.27	3.58	3.39	3.68	3.52	3.73	3.72	3.88	4.05
	50	3.37	3.76	3.60	3.52	3.68	3.47	3.78	3.89	4.09	3.96	4.16	4.34	4.24
10.0mm/1i	25	2.71	2.76	2.72	2.94	3.01	3.06	3.00	3.13	3.35	3.52	3.22	3.42	3.60
	50	2.88	3.10	3.15	3.21	3.00	3.19	3.36	3.15	3.46	3.61	3.56	3.68	3.70
10.0mm/2i	25	2.67	2.75	2.84	2.73	3.17	2.78	2.93	3.02	3.25	3.32	3.30	3.30	3.48
	50	3.13	2.86	3.12	2.86	3.00	3.02	3.18	3.41	3.53	3.56	3.83	3.54	3.70

Table 11. Varied parameters and standard deviation (SD) of water with ROI area 1000 mm^2, body.

Thickness/ Speed/Pitch	SFOV/DFOV (cm)	mA										
		240	230	220	210	200	190	180	170	160	150	140
1.25/3.75/0.75	50/35	10.36	10.72	10.94	10.72	11.29	11.28	11.52	12.28	12.90	12.87	13.46
	25/25	9.27	9.85	10.15	10.27	10.89	11.16	10.93	11.69	11.43	12.03	12.98
1.25/7.50/1.5	50/35	12.56	12.79	12.43	13.00	13.50	13.06	14.49	13.91	14.98	15.13	16.02
	25/25	10.82	10.85	11.70	11.99	12.17	12.49	12.82	13.21	13.87	14.48	14.83
2.50/3.75/0.75	50/35	6.76	6.58	6.63	6.65	6.99	7.75	7.55	7.79	8.03	7.95	8.79
	25/25	6.03	6.18	6.10	6.36	6.64	6.81	6.95	7.40	7.10	7.85	7.88
2.50/7.50/0.75	50/35	7.36	7.40	7.59	7.78	7.82	8.58	8.34	8.84	9.19	9.08	9.47
	25/25	6.60	7.11	7.01	7.32	7.54	7.59	7.94	8.07	8.55	8.51	8.96
2.50/7.50/1.5	50/35	8.44	9.14	9.14	9.94	9.97	10.11	9.93	10.45	11.04	11.41	12.46
	25/25	8.27	8.35	8.99	9.16	9.47	9.40	9.84	10.11	10.70	10.54	10.75
2.50/15.00/1.5	50/35	8.75	8.97	9.00	9.20	9.30	9.46	9.71	9.97	10.54	10.89	11.32
	25/25	7.85	8.16	7.91	8.26	8.46	9.08	9.02	9.75	9.72	10.01	9.96
3.75/7.50/0.75	50/35	5.03	5.29	5.38	5.66	5.69	5.93	6.09	6.15	6.28	6.69	6.86
	25/25	4.73	4.82	5.17	5.21	5.50	5.53	5.57	5.65	5.84	6.14	6.48
3.75/11.25/0.75	50/35	5.82	6.09	6.01	6.39	6.56	6.46	6.79	7.15	7.31	7.30	7.26
	25/25	5.56	5.72	5.78	5.84	6.27	6.26	6.54	6.32	6.82	7.10	7.12
3.75/15.00/1.5	50/35	7.45	7.53	7.60	7.90	8.29	8.12	8.92	8.84	9.17	9.56	9.96
	25/25	6.68	7.01	7.17	7.30	7.73	7.84	7.92	8.23	8.46	9.15	9.04
5.0/7.50/0.75	50/35	4.56	4.65	4.72	4.89	5.15	5.17	5.16	5.34	5.42	5.78	5.51
	25/25	4.12	4.49	4.53	4.80	4.84	4.88	5.07	5.07	5.07	5.34	5.65
5.0/11.25/0.75	50/35	4.48	4.80	4.81	4.83	5.27	4.98	5.12	5.34	5.66	5.75	5.99
	25/25	4.37	4.37	4.57	4.57	4.92	4.94	5.10	5.14	5.45	5.36	5.58
5.0/15.00/0.75	50/35	5.03	5.23	4.94	5.22	5.31	5.67	5.86	5.98	6.53	6.25	6.57
	25/25	4.77	4.79	4.99	4.99	5.30	5.55	5.78	5.41	5.97	6.19	6.14
5.0/15.00/1.5	50/35	6.21	6.33	6.95	6.59	6.99	6.88	7.23	7.67	7.79	8.26	8.47
	25/25	6.10	6.00	6.19	6.33	6.43	6.70	6.80	7.21	7.18	7.35	7.73
5.0/22.50/1.5	50/35	5.29	5.68	5.74	6.09	6.17	6.35	6.54	6.74	6.80	7.05	7.33
	25/25	5.14	5.47	5.35	5.51	5.72	6.25	6.16	6.36	6.52	6.86	6.96
5.0/30.00/1.5	50/35	5.87	6.02	6.02	6.27	6.54	6.73	6.76	7.00	7.08	7.55	7.40
	25/25	5.33	5.44	5.68	5.93	5.75	6.61	6.35	6.58	6.48	6.77	7.29
7.5/11.25/0.75	50/35	3.72	3.82	3.94	3.77	3.95	4.09	4.25	4.41	4.24	4.55	4.85
	25/25	3.56	3.53	3.67	3.67	3.91	3.99	3.95	4.16	4.21	4.22	4.50
7.5/15.00/0.75	50/35	3.54	3.70	3.85	3.89	3.92	4.11	4.17	4.17	4.28	4.25	4.57
	25/25	3.56	3.65	3.46	3.56	3.68	3.89	4.09	4.09	4.13	4.22	4.48
7.5/22.50/1.5	50/35	5.02	5.26	5.49	5.40	5.47	5.69	5.59	6.06	6.34	6.49	6.82
	25/25	4.59	5.04	5.19	5.34	5.60	5.41	5.70	5.78	6.18	6.09	6.49
7.5/30.00/1.5	50/35	5.15	5.24	5.44	5.52	5.55	5.91	6.09	6.28	6.45	6.49	6.58

Table 11. Varied parameters and standard deviation (SD) of water with ROI area 1000 mm^2, body. (Continued)

Thickness/ Speed/Pitch	SFOV/DFOV (cm)	mA										
		240	230	220	210	200	190	180	170	160	150	140
10.0/15.00/0.75	25/25	4.92	4.99	4.76	5.16	5.28	5.64	5.74	5.87	5.92	6.21	6.48
	50/35	3.23	3.27	3.40	3.40	3.48	3.40	3.72	3.72	3.86	3.96	4.26
10.0/30.00/1.5	25/25	3.08	3.09	3.13	3.25	3.35	3.30	3.58	3.52	3.65	3.71	3.93
	50/35	4.44	4.50	4.55	4.77	4.89	4.96	5.08	5.40	5.57	5.53	5.60
	25/25	4.32	4.13	4.34	4.42	4.64	4.87	4.98	5.07	5.33	5.23	5.65

Table 12. Varied parameters and DLP_{air} of head posterior fossa and above.

Posterior fossa			mA										
Thickness	Scan length/ Image	SFOV (cm)	160	155	150	145	140	135	130	125	120	115	110
1.25 mm/4i	S0-S48.75	25	634.29	615.07	596.30	576.03	557.11	536.55	517.77	497.36	477.39	458.02	437.46
	40i	50	525.22	509.13	493.63	476.80	459.66	444.32	427.33	410.34	395.00	377.71	360.73
2.50 mm/2i	S0-S48.76	25	644.12	623.41	601.51	581.10	562.17	541.61	521.35	500.94	481.86	461.45	441.04
	40i	50	531.48	514.35	498.40	481.42	464.88	447.89	430.76	413.62	398.13	380.25	364.15
2.50 mm/4i	S0-S48.77	25	495.72	480.22	464.88	449.38	432.69	418.84	402.60	386.50	371.01	355.51	339.87
	40i	50	410.20	397.23	384.72	371.16	359.09	345.53	333.31	319.75	307.83	294.27	282.20
3.75 mm/4i	S0-S48.78	25	450.57	436.12	422.26	408.56	395.00	381.14	367.28	352.23	338.68	324.97	309.62
	40i	50	373.54	361.32	350.45	337.19	326.46	313.64	302.77	290.25	278.93	266.86	255.09

Above			140	135	130	125	120	115	110	105	100
5.00 mm/1i	S50-S115	25	22.66	21.93	21.37	20.47	19.53	18.64	17.88	17.34	16.45
	14i	50	19.49	18.77	18.06	17.39	16.90	16.23	15.56	14.80	14.10
5.00 mm/2i	S50-S115	25	17.39	17.03	16.40	15.73	15.11	14.53	14.20	13.28	12.61
	14i	50	15.06	14.48	13.99	13.45	12.92	12.38	11.85	11.31	10.73
5.00 mm/4i	S50-S105	25	12.98	12.53	12.09	11.64	11.19	10.75	10.30	9.81	9.32
	12i	50	11.02	10.84	10.44	10.03	9.68	9.23	8.83	8.47	8.03
7.50 mm/2i	S50-S117.5	25	23.67	22.92	22.08	21.27	20.43	19.62	18.78	17.93	17.17
	10i	50	20.16	19.44	18.78	17.97	17.30	16.68	16.01	15.89	14.54
10.0 mm/1i	S50-S120	25	31.89	30.77	29.63	28.50	27.43	26.36	25.26	24.08	22.92
	8i	50	26.98	26.00	25.06	24.08	23.15	22.21	21.23	20.25	19.31
10.0 mm/2i	S50-S120	25	28.79	27.90	26.91	25.79	24.85	23.82	22.75	21.75	20.72
	8i	50	24.39	23.55	22.66	21.76	20.91	20.06	19.21	18.27	17.42

Table 13. Varied parameters and DLP_{air} of body pre-contrast.

Thickness/ Speed/Pitch	SFOV/ DFOV (cm)	mA										
		240	230	220	210	200	190	180	170	160	150	140
5.0/7.50/0.75	50/35	759.40	731.40	698.53	666.69	599.92	571.03	541.84	510.59	480.38	451.19	421.86
	25/25	914.76	875.41	839.59	800.23	718.87	685.12	647.97	611.86	576.04	540.22	505.43
5.0/11.25/0.75	50/35	691.90	663.45	642.81	612.15	580.61	551.28	510.30	481.70	452.96	415.96	389.58
	25/25	832.96	796.70	772.08	736.41	697.35	661.38	614.66	579.28	545.53	500.28	467.41
5.0/15.00/0.75	50/35	667.87	637.80	608.32	580.61	522.98	495.26	470.06	442.79	416.99	380.88	355.23
	25/25	802.00	766.19	732.28	698.53	627.04	595.05	565.43	533.29	502.34	457.53	425.84
5.0/15.00/1.5	50/35	375.28	360.10	354.94	338.58	290.67	276.23	260.16	246.01	230.98	209.75	195.01
	25/25	451.19	432.32	427.17	406.97	348.75	332.09	313.08	295.98	278.88	252.05	234.37
5.0/22.50/1.5	50/35	346.54	333.12	321.63	307.03	291.56	277.11	253.23	239.53	225.67	213.73	199.43
	25/25	416.99	399.90	386.78	369.53	349.49	332.53	305.71	289.05	271.95	256.62	239.53
5.0/30.00/1.5	50/35	334.01	320.45	305.27	292.00	262.52	249.55	233.33	220.81	207.24	193.09	180.12
	25/25	401.67	384.86	366.88	350.37	315.14	299.22	281.30	265.17	249.70	231.86	216.53
7.5/11.25/0.75	50/35	691.75	663.45	641.34	610.24	580.61	551.57	510.89	481.41	453.26	420.97	393.26
	25/25	830.45	798.76	771.79	733.90	697.20	663.01	614.95	577.66	545.09	506.32	471.68
7.5/15.00/0.75	50/35	666.54	639.42	608.91	581.35	522.98	496.30	470.06	442.64	415.37	383.24	356.27
	25/25	799.50	768.40	731.99	698.97	627.63	596.09	565.57	532.11	500.57	460.33	427.75
7.5/22.50/1.5	50/35	346.83	333.12	321.04	307.33	291.85	277.70	253.97	239.38	224.20	214.61	200.17
	25/25	416.70	400.04	386.04	369.24	350.22	332.83	306.00	287.43	270.33	258.54	240.11
7.5/30.00/1.5	50/35	334.01	321.04	304.97	292.59	262.81	244.68	233.48	219.33	207.10	194.42	181.15
	25/25	401.67	386.04	366.88	351.25	315.44	294.80	281.39	265.17	248.37	233.63	217.86
10.0/15.00/0.75	50/35	663.45	639.57	609.20	582.67	523.12	493.50	469.91	442.64	416.26	385.89	359.36
	25/25	798.76	769.28	731.40	700.00	628.22	593.58	564.39	533.29	500.57	462.54	431.15
10.0/30.00/1.5	50/35	334.16	321.04	305.27	292.88	263.26	244.83	232.89	220.81	207.24	194.72	182.04
	25/25	401.67	385.45	366.58	351.40	315.44	295.68	280.65	265.03	249.40	233.78	218.15

Table 14. Varied parameters and DLP_{air} of body post-contrast.

Thickness Speed/Pitch	SFOV/ DFOV (cm)	mA										
		240	230	220	210	200	190	180	170	160	150	140
1.25/3.75/0.75	50/35	569.11	544.05	508.97	486.71	418.62	398.27	378.52	357.30	335.34	313.81	295.39
	25/25	683.05	656.37	613.77	584.74	503.67	479.20	455.02	428.79	403.73	378.08	355.82
1.25/7.50/1.5	50/35	289.94	276.08	259.28	245.57	211.22	203.26	192.65	180.86	169.95	159.34	149.02
	25/25	348.31	332.83	310.28	297.45	254.71	243.65	231.71	218.74	206.21	192.50	179.53
2.50/3.75/0.75	50/35	574.71	550.69	514.13	491.14	423.19	401.37	382.65	361.28	339.76	316.91	299.37
	25/25	688.80	662.42	620.85	574.27	510.59	483.77	461.80	434.68	408.89	381.18	360.39
2.50/7.50/0.75	50/35	437.63	419.50	402.25	373.07	336.51	320.89	306.59	289.20	271.22	253.68	240.56
	25/25	526.81	505.88	484.80	449.13	404.91	386.04	368.06	348.01	326.05	304.82	288.61
2.50/7.50/1.5	50/35	295.09	281.24	263.85	243.95	215.50	206.21	196.19	184.40	172.61	161.55	152.26
	25/25	353.76	338.58	317.94	293.92	259.13	248.81	235.84	223.16	208.72	195.16	183.22
2.50/15.00/1.5	50/35	226.55	216.09	207.83	192.50	173.93	164.50	157.13	148.43	139.15	130.45	123.08
	25/25	272.69	260.60	249.25	231.86	207.69	198.99	188.97	178.06	167.59	157.13	147.99
3.75/7.50/0.75	50/35	442.64	423.92	404.91	376.61	339.76	322.66	308.36	289.94	274.02	255.89	243.36
	25/25	533.59	509.56	487.89	452.52	408.59	389.43	371.01	348.01	329.14	308.21	291.70
3.75/11.25/0.75	50/35	427.17	408.30	390.76	364.37	357.30	341.23	323.99	304.09	287.28	269.30	254.85
	25/25	512.95	492.76	471.09	438.52	430.70	409.92	389.58	365.40	345.36	323.84	305.71
3.75/15.00/1.5	50/35	229.94	221.39	211.22	195.75	177.17	167.74	160.22	150.05	141.95	133.10	124.55
	25/25	276.08	266.06	253.38	235.69	211.22	203.41	193.98	180.71	170.69	159.93	149.61
5.0/7.50/0.75	50/35	446.03	428.93	409.62	381.62	343.44	327.67	312.78	293.18	277.11	259.28	244.24
	25/25	537.13	515.31	493.35	459.00	413.46	394.59	375.58	353.02	333.12	311.75	293.47
5.0/11.25/0.75	50/35	427.31	409.92	392.08	364.52	357.74	341.67	324.57	304.97	287.58	279.77	254.27
	25/25	513.10	492.32	471.24	438.52	430.41	411.84	390.32	366.44	345.21	336.07	305.56
5.0/15.00/0.75	50/35	432.32	413.01	395.47	369.53	337.25	323.84	306.74	288.61	271.22	261.05	240.56
	25/25	519.29	497.48	476.25	443.67	404.91	389.14	368.79	346.68	326.05	313.81	288.31
5.0/15.00/1.5	50/35	234.37	224.64	213.44	199.14	179.24	170.54	162.43	153.00	143.86	135.61	126.47
	25/25	281.39	270.63	257.80	240.11	214.02	205.92	196.48	183.66	173.05	163.17	152.12
5.0/22.50/1.5	50/35	230.09	221.25	210.93	195.89	190.44	182.78	173.20	163.17	153.89	145.34	135.61
	25/25	277.70	266.20	253.68	237.17	230.09	221.25	209.46	197.52	185.28	174.82	163.17
5.0/30.00/1.5	50/35	228.76	219.63	209.16	195.16	178.80	169.66	160.67	151.53	143.13	134.58	125.73
	25/25	276.08	264.14	251.17	235.40	213.14	205.92	194.42	182.19	171.87	161.55	150.94

Table 15. Radiation dose characteristics with depend on the total nominal scan width in axial mode (25 cm SFOV).

Posterior fossa			mA										
Head mode	Total nominal scan width (mm)	Slice thickness (mm)	160	155	150	145	140	135	130	125	120	115	110
2i	5	2.50	644.12	623.41	601.51	581.10	562.17	541.61	521.35	500.94	481.86	461.45	441.04
4i	5	1.25	634.29	615.07	596.30	576.03	557.11	536.55	517.77	497.36	477.39	458.02	437.46
4i	10	2.50	495.72	480.22	464.88	449.38	432.69	418.84	402.60	386.50	371.01	355.51	339.87
4i	15	3.75	450.57	436.12	422.26	408.56	395.00	381.14	367.28	352.23	338.68	324.97	309.62
Above posterior fossa			140	135	130	125	120	115	110	105	100		
1i	5	5.00	22.66	21.93	21.37	20.47	19.53	18.64	17.88	17.34	16.45		
1i	10	10.0	31.89	30.77	29.63	28.50	27.43	26.36	25.26	24.08	22.92		
2i	10	5.00	17.39	17.03	16.40	15.73	15.11	14.53	14.20	13.28	12.61		
2i	15	7.50	23.67	22.92	22.08	21.27	20.43	19.62	18.78	17.93	17.17		
2i	20	10.0	28.79	27.90	26.91	25.79	24.85	23.82	22.75	21.75	20.72		
4i	20	5.00	12.98	12.53	12.09	11.64	11.19	10.75	10.30	9.81	9.32		

Table 16. Radiation dose characteristics with depend on the total nominal scan width in axial mode (50 cm SFOV).

Posterior fossa			mA										
Head mode	Total nominal scan width (mm)	Slice thickness (mm)	160	155	150	145	140	135	130	125	120	115	110
2i	5	2.50	531.48	514.35	498.40	481.42	464.88	447.89	430.76	413.62	398.13	380.25	364.15
4i	5	1.25	525.22	509.13	493.63	476.80	459.66	444.32	427.33	410.34	395.00	377.71	360.73
4i	10	2.50	410.20	397.23	384.72	371.16	359.09	345.53	333.31	319.75	307.83	294.27	282.20
4i	15	3.75	373.54	361.32	350.45	337.19	326.46	313.64	302.77	290.25	278.93	266.86	255.09
Above posterior fossa			140	135	130	125	120	115	110	105	100		
1i	5	5.00	19.49	18.77	18.06	17.39	16.90	16.23	15.56	14.80	14.10		
1i	10	10.0	26.98	26.00	25.06	24.08	23.15	22.21	21.23	20.25	19.31		
2i	10	5.00	15.06	14.48	13.99	13.45	12.92	12.38	11.85	11.31	10.73		
2i	15	7.50	20.16	19.44	18.78	17.97	17.30	16.68	16.01	15.89	14.54		
2i	20	10.0	24.39	23.55	22.66	21.76	20.91	20.06	19.21	18.27	17.42		
4i	20	5.00	11.02	10.84	10.44	10.03	9.68	9.23	8.83	8.47	8.03		

Table 17. Radiation dose characteristics with depend on the total nominal scan width in helical mode (body pre-contrast, 25 cm SFOV).

Body mode	Table speed (mm per - rotation)	Total nominal scan width (mm)	Slice thickness (mm)	mA										
				240	230	220	210	200	190	180	170	160	150	140
HQ	7.50	10	5.0	914.76	875.41	839.59	800.23	718.87	685.12	647.97	611.86	576.04	540.22	505.43
	11.25	15	5.0	832.96	796.70	772.08	736.41	697.35	661.38	614.66	579.28	545.53	500.28	467.41
	11.25	15	7.5	830.45	798.76	771.79	733.90	697.20	663.01	614.95	577.66	545.09	506.32	471.68
	15.00	20	5.0	802.00	766.19	732.28	698.53	627.04	595.05	565.43	533.29	502.34	457.53	425.84
	15.00	20	7.5	799.50	768.40	731.99	698.97	627.63	596.09	565.57	532.11	500.57	460.33	427.75
	15.00	20	10.0	798.76	769.28	731.40	700.00	628.22	593.58	564.39	533.29	500.57	462.54	431.15
HS	15.00	10	5.0	451.19	432.32	427.17	406.97	348.75	332.09	313.08	295.98	278.88	252.05	234.37
	22.50	15	5.0	416.99	399.90	386.78	369.53	349.49	332.53	305.71	289.05	271.95	256.62	239.53
	22.50	15	7.5	416.70	400.04	386.04	369.24	350.22	332.83	306.00	287.43	270.33	258.54	240.11
	30.00	20	5.0	401.67	384.86	366.88	350.37	315.14	299.22	281.30	265.17	249.70	231.86	216.53
	30.00	20	7.5	401.67	386.04	366.88	351.25	315.44	294.80	281.39	265.17	248.37	233.63	217.86
	30.00	20	10.0	401.67	385.45	366.58	351.40	315.44	295.68	280.65	265.03	249.40	233.78	218.15

Table 18. Radiation dose characteristics with depend on the total nominal scan width in helical mode (body pre-contrast, 50 cm SFOV).

Body mode	Table speed (mm per - rotation)	Total nominal scan width (mm)	Slice thickness (mm)	mA										
				240	230	220	210	200	190	180	170	160	150	140
HQ	7.50	10	5.0	759.40	731.40	698.53	666.69	599.92	571.03	541.84	510.59	480.38	451.19	421.86
	11.25	15	5.0	691.90	663.45	642.81	612.15	580.61	551.28	510.30	481.70	452.96	415.96	389.58
	11.25	15	7.5	691.75	663.45	641.34	610.24	580.61	551.57	510.89	481.41	453.26	420.97	393.26
	15.00	20	5.0	667.87	637.80	608.32	580.61	522.98	495.26	470.06	442.79	416.99	380.88	355.23
	15.00	20	7.5	666.54	639.42	608.91	581.35	522.98	496.30	470.06	442.64	415.37	383.24	356.27
	15.00	20	10.0	663.45	639.57	609.20	582.67	523.12	493.50	469.91	442.64	416.26	385.89	359.36
HS	15.00	10	5.0	375.28	360.10	354.94	338.58	290.67	276.23	260.16	246.01	230.98	209.75	195.01
	22.50	15	5.0	346.54	333.12	321.63	307.03	291.56	277.11	253.23	239.53	225.67	213.73	199.43
	22.50	15	7.5	346.83	333.12	321.04	307.33	291.85	277.70	253.97	239.38	224.20	214.61	200.17
	30.00	20	5.0	334.01	320.45	305.27	292.00	262.52	249.55	233.33	220.81	207.24	193.09	180.12
	30.00	20	7.5	334.01	321.04	304.97	292.59	262.81	244.68	233.48	219.33	207.10	194.42	181.15
	30.00	20	10.0	334.16	321.04	305.27	292.88	263.26	244.83	232.89	220.81	207.24	194.72	182.04

Table 19. Radiation dose characteristics with depend on the total nominal scan width in helical mode (body post-contrast, 25 cm SFOV).

Body mode	Table speed (mm per - rotation)	Total nominal scan width (mm)	Slice thickness (mm)	mA										
				240	230	220	210	200	190	180	170	160	150	140
HQ	3.75	5	1.25	683.05	656.37	613.77	584.74	503.67	479.20	455.02	428.79	403.73	378.08	355.82
	3.75	5	2.50	688.80	662.42	620.85	574.27	510.59	483.77	461.80	434.68	408.89	381.18	360.39
	7.50	10	2.50	526.81	505.88	484.80	449.13	404.91	386.04	368.06	348.01	326.05	304.82	288.61
	7.50	10	3.75	533.59	509.56	487.89	452.52	408.59	389.43	371.01	348.01	329.14	308.21	291.70
	7.50	10	5.0	537.13	515.31	493.35	459.00	413.46	394.59	375.58	353.02	333.12	311.75	293.47
	11.25	15	3.75	512.95	492.76	471.09	438.52	430.70	409.92	389.58	365.40	345.36	323.84	305.71
	11.25	15	5.0	513.10	492.32	471.24	438.52	430.41	411.84	390.32	366.44	345.21	336.07	305.56
	15.00	20	5.0	519.29	497.48	476.25	443.67	404.91	389.14	368.79	346.68	326.05	313.81	288.31
HS	7.50	5	1.25	348.31	332.83	310.28	297.45	254.71	243.65	231.71	218.74	206.21	192.50	179.53
	7.50	5	2.50	353.76	338.58	317.94	293.92	259.13	248.81	235.84	223.16	208.72	195.16	183.22
	15.00	10	2.50	272.69	260.60	249.25	231.86	207.69	198.99	188.97	178.06	167.59	157.13	147.99
	15.00	10	3.75	276.08	266.06	253.38	235.69	211.22	203.41	193.98	180.71	170.69	159.93	149.61
	15.00	10	5.0	281.39	270.63	257.80	240.11	214.02	205.92	196.48	183.66	173.05	163.17	152.12
	22.50	15	5.0	277.70	266.20	253.68	237.17	230.09	221.25	209.46	197.52	185.28	174.82	163.17
	30.00	20	5.0	276.08	264.14	251.17	235.40	213.14	205.92	194.42	182.19	171.87	161.55	150.94

Table 20. Radiation dose characteristics with depend on total nominal scan width in helical mode (body post-contrast, 50 cm SFOV).

Body mode	Table speed (mm per - rotation)	Total nominal scan width (mm)	Slice thickness (mm)	mA										
				240	230	220	210	200	190	180	170	160	150	140
HQ	3.75	5	1.25	569.11	544.05	508.97	486.71	418.62	398.27	378.52	357.30	335.34	313.81	295.39
	3.75	5	2.50	574.71	550.69	514.13	491.14	423.19	401.37	382.65	361.28	339.76	316.91	299.37
	7.50	10	2.50	437.63	419.50	402.25	373.07	336.51	320.89	306.59	289.20	271.22	253.68	240.56
	7.50	10	3.75	442.64	423.92	404.91	376.61	339.76	322.66	308.36	289.94	274.02	255.89	243.36
	7.50	10	5.0	446.03	428.93	409.62	381.62	343.44	327.67	312.78	293.18	277.11	259.28	244.24
	11.25	15	3.75	427.17	408.30	390.76	364.37	357.30	341.23	323.99	304.09	287.28	269.30	254.85
	11.25	15	5.0	427.31	409.92	392.08	364.52	357.74	341.67	324.57	304.97	287.58	279.77	254.27
	15.00	20	5.0	432.32	413.01	395.47	369.53	337.25	323.84	306.74	288.61	271.22	261.05	240.56
HS	7.50	5	1.25	289.94	276.08	259.28	245.57	211.22	203.26	192.65	180.86	169.95	159.34	149.02
	7.50	5	2.50	295.09	281.24	263.85	243.95	215.50	206.21	196.19	184.40	172.61	161.55	152.26
	15.00	10	2.50	226.55	216.09	207.83	192.50	173.93	164.50	157.13	148.43	139.15	130.45	123.08
	15.00	10	3.75	229.94	221.39	211.22	195.75	177.17	167.74	160.22	150.05	141.95	133.10	124.55
	15.00	10	5.0	234.37	224.64	213.44	199.14	179.24	170.54	162.43	153.00	143.86	135.61	126.47
	22.50	15	5.0	230.09	221.25	210.93	195.89	190.44	182.78	173.20	163.17	153.89	145.34	135.61
	30.00	20	5.0	228.76	219.63	209.16	195.16	178.80	169.66	160.67	151.53	143.13	134.58	125.73

CHAPTER VI
DISCUSSIONS

6.1 Optimization of scan parameters

Efficient optimization of imaging parameters to minimize x-ray exposure is possible only if the radiation dose response characteristics of a multi-detector CT scanner are known. Carefully of scanning parameters selection is the essential in an optimization process because it is effect on both image quality and dose. From our results, the following are the suggestions of each scan parameter on how to optimize multi-detector scanning.

6.1.1 Tube current (mA)

In theory, increasing tube current is directly proportional to an increase in dose. A reduction of tube current reduces image quality along with dose. Thus a careful balance is needed to ensure that the necessary diagnostic information is obtained.

Our results showed that, tube current can be reduced approximately 38% (from 160 to 100 mA) in head protocol and 42% (from 240 to 140 mA) in body protocol without any degradation of spatial resolution. Our results agreed with previous investigation that, in areas of high natural contrast, such as the chest or skeleton, image noise is less critical and clinically acceptable images can be obtained with reduced tube current

However, any decrease in tube current should be considered carefully, because such reduction causes an increase in image noise, which may affect the diagnostic outcome of the examination. This is especially true in areas where low contrast is severely affected by an increase in image noise, such as in abdominal studies.

6.1.2 Slice thickness

Acquired slice thickness has an important relationship to dose. The dose efficiency of multi-detector CT scanning diminishes with very thin slices because the penumbra, the unused portion of the x-ray beam that lands outside the active portion of the detector's array, becomes a much larger fraction of the total dose profile with very thin slices and thus increasing dose (52). As seen in the results of this study and is discussed below.

In axial mode, there was a relative increase in the size of the penumbra of the radiation beam in the 1i mode. This penumbra did not contribute to image generation but to dose. The penumbral effect in multi-detector CT could be minimized by imaging with a radiation beam with the widest available nominal x-ray beam width (2i or 4i mode). As an example, a head above posterior fossa protocol was performed with 140 mA 25 cm SFOV and 5 mm thickness 1i mode and resulted in radiation dose of 22.6 mGy.cm. After optimization to 2i and 4i mode, the multi-detector protocols would result in a dose of 17.39 and 12.98 mGy.cm, respectively. These optimizations could result in dose reduction of 23% and 25%, respectively.

Similar result in a head posterior fossa protocol that performed with 160 mA 25 cm SFOV and 2.5 mm thickness 2i mode was found and resulted in radiation dose of 644.12 mGy.cm. After optimization to 4i mode, the multi-detector protocols would result in a dose of 495.72 mGy.cm, which was 23% of dose reduction.

From this reason, one should choose the minimal slice thickness before the penumbra dose penalty becomes significant. Otherwise, scanning should be made with medium or wide collimation and 4i mode should be employed instead of the 1i or 2i mode.

Other findings demonstrated that at the same nominal scan width a change in the slice thickness did not change the radiation dose. This suggested that it was an inherent property of the scanner model. From this reason, thinner or thicker slice thickness can be selected to provide desired image quality. When thicker slice thickness is chosen in order to reduce image noise and improve low contrast resolution, spatial resolution will be compromised by partial volume effect. By contrast, if a narrow slice thickness is used, the visibility of small details will be improved despite the increase of noise.

6.1.3 Pixel size

Our results showed that at two variation pixel sizes: 0.49 and 0.98 mm, pixel size was inversely related to dose and an increase in dose was observed when the change from the large to the small pixel size was made. For consideration of image quality, when other scan parameters are constant, only image noise is dependent on a change in pixel size whereas spatial resolution and low contrast resolution are relatively constant. We concluded from our results that, the 0.98 cm pixel size was the optimal value that could provide adequate image quality for general applications while maintaining low level of radiation dose.

6.1.4 Pitch

In theory, pitch is inversely related to dose, increasing the pitch diminishes the dose and diminishing the pitch increases the dose. Our results indicated that, the 0.75 helical pitch was suitable for those applications demanding good contrast resolution and low image noise. For applications required high volume coverage speed in thin slice scan, good temporal resolution and minimization of motion blurring, pitch of 1.5 was appropriate.

Although scanning at a higher pitch is generally more dose efficient, it also tends to cause increasable in noise and decrease in low contrast resolution. Hence, alterations in pitch can have varying effects on image quality in different situations.

6.2 Dose optimization

Optimization of dose can be achieved by focusing on image quality, which can be adjusted by appropriate selection of scanning parameters in routine clinical practice. Optimal scanning parameters for different clinical protocols are shown as the followings;

6.2.1 Standard techniques

Head posterior fossa:	160 mA, 2.5mm(2i) slice thickness, 25 cm SFOV (0.49 mm pixel size)
Head above posterior fossa:	140 mA, 7.5mm(2i) slice thickness, 25 cm SFOV (0.49 mm pixel size)
Body pre-contrast:	200 mA, 10.0/15.00 slice thickness/table speed, pitch 0.75, 50 cm SFOV (0.98 mm pixel size)
Body post-contrast:	220 mA, 3.75/11.25 slice thickness/table speed, pitch 0.75, 50 cm SFOV (0.98 mm pixel size)

6.2.2 Dose optimization of a multi-detector CT in comparison with the standard technique

6.2.2.1 Dose versus Spatial resolution

Our results showed that spatial resolution was minimally affected from the variation of scanning parameters. Thus, dose can be reduced approximately 60% (from 644.12 to 255.09 mGy.cm) in head posterior fossa protocol, 66% (from 23.67 to 8.03 mGy.cm) in head above posterior fossa protocol, 66% (from 523.12 to 180.12 mGy.cm) in body pre-contrast protocol, 69% (from 390.76 to 123.08 mGy.cm) in body post-contrast protocol, at the maximum of dose reduction with all scan protocols are consider, without any degradation of spatial resolution.

6.2.2.2 Dose versus Low contrast resolution

From our results, main scanning parameters that affect to low contrast resolution was slice thickness. This was because radiation dose from multi-detector CT scan was affected by the nominal scan width, not the reconstructed slice thickness.

Thus the different from single-detector CT is that, in the same total nominal scan width (proximally dose), multi-detector CT can improve low contrast resolution by increase slice thickness and do not increase dose. Example of the above finding is, in body pre-contrast protocol (230 mA, HQ mode, 0.98 mm pixel size, 20 mm total nominal scan width and acquire slice thickness are 5.0, 7.5 and 10.0 mm), can improve low contrast resolution (from 28.5, 32.0 to 34.0, respectively) by increase slice thickness with do not increase dose (637.80, 639.42 and 639.57 mGy.cm, respectively).

Radiation dose can be reduced in proportion to reduction in mAs, but image noise can be increased in proportion to $\sqrt{(mAs_{original})/(mAs_{reduced})}$. Therefore, if the mAs is reduced to ½ of the original, then the noise is expected to increase by 1.41 (41% increase) and this should degrade the low contrast resolution performance (25).

In this study, at the maximum of tube current reduction from 160 to 110 mA in head posterior fossa protocol, from 140 to 100 mA in head above posterior fossa protocol, from 200 to 140 mA in body pre-contrast protocol and from 220 to 140 in body post-contrast protocol, image noise from calculation was increased to 21%, 18%, 20% and 25%, respectively. From IPEM Report No. 77 suggested tolerances and remedial levels of image noise (SD) is ± 20%, thus noise levels from reduced tube current in head above posterior fossa and body pre-contrast protocols are acceptable. But in head posterior fossa and body post-contrast protocols, noise levels are unacceptable and thus minimal value of tube current reduction which acceptable noise level in each protocol is 115 mA and 160 mA (or over 150 mA), respectively.

Therefore, when reduce tube current to the minimum value, dose reduction in each protocols were about 28% (from 644.12 (160 mA) to 461.45 (115 mA) mGy.cm) in head posterior fossa protocol, 27% (from 23.67 (140 mA) to 17.17 (100 mA) mGy.cm) in head above posterior fossa protocol, 31% (from 523.12 (200 mA) to

359.36 (140 mA) mGy.cm) in body pre-contrast protocol, 26% (from 390.76 (220 mA) to 287.28 (160 mA) mGy.cm) in body post-contrast protocol.

In body protocols, low contrast score was slightly dependent on pitch in thick slice thickness (7.5 and 10.0 mm); in thin slice thickness (1.25, 2.5, 3.75 and 5.0 mm) pitch selection did not affect low contrast score. Therefore in thin slice thickness dose can be reduced approximately 50% from 0.75 pitch to 1.5 pitch.

Pixel size selection did not affect to low contrast score in all examination protocols. Thus in head protocols that usually used small pixel size, when the change to the large pixel size was made dose can be reduced approximately 17% (from 644.12 to 531.48 mGy.cm) in head posterior fossa protocol and 15% (from 23.67 to 20.16 mGy.cm) in head above posterior fossa protocol.

6.2.2.3 Dose versus Noise

From our study indicated that image noise was the important factors affecting CT image quality. Variation of scanning parameters had an effect on image noise. When image noise was compared with the variation of each scanning parameters, we found that slice thickness is the main parameter that affect to noise. The latter parameters are tube current, pitch and pixel size, respectively.

In slice thickness scanning parameter, like low contrast resolution, image noise can decrease by increase slice thickness without increase in dose. For example, in body post-contrast protocol (150 mA, HS mode, 0.49 mm pixel size, 10 mm total nominal scan width and acquire slice thickness are 2.5, 3.75 and 5.0 mm), can reduce image noise (from 10.01, 9.15 to 7.35, respectively) by increase slice thickness without increase the dose (157.13, 159.93 and 163.17 mGy.cm, respectively).

In both head and body protocols when reduce tube current to the minimum value, where increase image noise about 15% (from 5.86 to 6.76), 24% (from 3.27 to 4.05), 22% (from 3.48 to 4.26) and 21% (from 6.01 to 7.26) in each above protocols respectively. Measuring noise levels from this reduced tube current were rather

acceptable. However, with the less tube current reduction values, low image noise is achieved. Thus minimal value of tube current reduction which acceptable noise level in head above posterior fossa, body pre-contrast and body post-contrast protocols were 105 mA, 150 mA and 170 mA, respectively.

When reduce tube current to the minimum value, dose reduction in each protocols were approximately 32% (from 644.12 (160 mA) to 441.04 (110 mA) mGy.cm) in head posterior fossa protocol, 24% (from 23.67 (140 mA) to 17.93 (105 mA) mGy.cm) in head above posterior fossa protocol, 26% (from 523.12 (200 mA) to 385.89 (150 mA) mGy.cm) in body pre-contrast protocol, 22% (from 390.76 (220 mA) to 304.09 (170 mA) mGy.cm) in body post-contrast protocol.

In addition, in image noise consideration when percentage of increased noise from measuring noise (SD) was compare with calculation noise (explain in part 6.2.2.2), we found the different from two methods. Maybe cause by ROI size selection that used in image analyzes process. However increased noise levels from both measuring and calculation were nearly, about 15 - 25%.

In body protocols, image noise was slightly dependent on pitch. When we changed to the high pitch, image noise was increase about 41% (from 3.48 to 4.89) in pre-contrast and 26% (from 6.01 to 7.60) in post-contrast with reduce dose about 50%. This should degrade the low contrast resolution performance.

In both head and body protocols, pixel size selection was minimally affect noise. Thus we can reduce dose in head protocols with the large pixel size selection approximately 17% (from 644.12 to 531.48 mGy.cm) in head posterior fossa protocol and 15% (from 23.67 to 20.16 mGy.cm) in head above posterior fossa protocol.

6.3 Other optimizations

6.3.1 Clinical aspects of setting the appropriate scan parameters

The scan parameters must be selected according to the area of examination and clinical indication in relation to the image quality and radiation dose to the patient. Such as, slice thickness is chosen according to the size of the anatomical structure or lesion that needs to be visualized, tube current is adjusted to patient size or an adequate of scan field of view (SFOV). If SFOV is too small, disease may be excluding from the visible image.

6.3.2 Compromising the scan parameters

Findings from our study indicated that image noise was the important factor affecting CT image quality. Noise is normally inversely related to the x-ray beam energy. Although decrease in tube current or increase in pixel size and pitch results in a reduction in radiation dose, such those are also associated with an increase in image noise. Therefore, in order to compensate for the increase the optimization process should compromise these scan parameters. For example, when the pitch selection is increased; a proportionate increase in tube current is made to maintain image quality. For narrow slice thickness the number of x-ray photons received at the detector is reduced and thus tube current is increased to maintain the signal to noise ratio in the image.

CHAPTER VII
CONCLUSION

In multi-detector CT, scanning parameters such as tube current, slice thickness, pixel size and pitch selection are factors affecting image quality and dose. From this study we found that for spatial resolution, changing imaging parameters did not affect much on the spatial resolution expect when the scan field of view was drastically increased. Our results suggested that dose reduction by adjusting scanning parameters from standard protocols can be achieved up to 60 - 69%.

For low contrast resolution and image noise, slice thickness was important factor controlling low contrast detectability. The thicker the slice, the better low contrast and noiseless could be observed. However, because radiation dose from multi-detector CT scan is affected by the nominal scan width, not the reconstructed slice thickness, in the same total nominal scan width (proximally dose), low contrast resolution can be improved by increase slice thickness without increasing the dose.

Tube current controls low contrast resolution and image noise. Acceptable noise level from minimal tube current value were 115 mA in head posterior fossa, 105 mA in head above posterior fossa, 150 mA in body pre-contrast and 170 mA in body post-contrast protocols. These optimal mA values provided about 22 - 28% of dose reduction as compared to standard scanning protocols.

Pixel size selection as a result from scan field of view and reconstruction matrix was another factor affecting the dose. However, pixel size does not affect low contrast resolution. Thus in head protocols, when compared to the standard practice and larger pixel was used, the dose was decreased approximately 15% and 17%.

Another concern is the pitch selection. We found that when the pitch was decreased from 1.5 to 0.75 to improve the contrast, the dose was doubled. In low contrast resolution, thin slice thickness (1.25, 2.5, 3.75 and 5.0 mm) pitch selection

did not affect low contrast score. And thus dose can be reduced approximately 50% from 0.75 pitch to 1.5 pitch.

Based on our study, to optimize image quality and dose in multi-detector scanning, a few rules for each scanning parameters could be summarized as the followings:

1. Tube current should be reduced to a minimum where possible, especially in high resolution studies. Tube current should be adjusted for specific patient sizes or anatomical regions.

2. Choose the minimal slice thickness before the penumbra dose penalty becomes significant.

3. A high pitch should be selected to preserve temporal resolution for moving organ imaging.

4. A large pixel size which provides enough image contrast should be selected.

These optimal scanning parameters should be selected and adjusted based on each patient, organ system, region scanned or clinical requirement.

In addition, this study provided a data set and tables of image quality and radiation dose as a function of the scanning parameters that can be applied or modified as the choice of user-selectable scan parameters for different clinical applications.

However, because the limitation of the phantom used in this study such as its size or it dose not consist of inner structure like in the actual patient, therefore, the results may not be directly transferable to in patient examination.

Future directions

This study was though performed on a phantom model. Based on our physical and dosimetric data, further clinical investigation in similar manner should be carried out to ensure the clinical quality of the CT images. Radiation dose to patients in term of effective dose, which represents stochastic risks from radiation, should also be assessed.

REFERENCES

1. Dawson P, Lees WR. Multi-slice technology in computed tomography. Clin Radiol 2001;56:302-9.
2. Rydberg J, Buckwalter KA, Caldemeyer KS, Philips MD, Conces DJ, Aisen AM, et al. Multisection CT: scanning techniques and clinical applications. Radiographics 2000;20:1787-806.
3. Barrett J. The new CT technology: what are the benefits? An invited lecture presented an UK radiology congress. London. 2002.
4. United Nations Scientific Committee on the Effects of Atomic Radiation. UNSCEAR 2000 Report to the General Assembly. Annex D: Medical radiation exposures. New York: United Nations; 2000.
5. Venema HW. Modulation transfer functions of single-slice and dual-slice computed tomography scanners. Med Phys 1996;23(11):1863-4.
6. Klingenbeck-Regn K, Schaller S, Flohr T, Ohnesorge B, Kopp AF, Baum U. Subsecond multi-slice computed tomography: basics and applications. Eur J Radiol 1999;31:110-24.
7. McCollough CH, Zink FE. Performance evaluation of a multi-slice CT system. Med Phys 1999;26(11):2223-30.
8. Albert T. LightSpeed QX/i. ELE Biomedical Engineering Seminar II, 2000. Available from: URL: http://www.ele.uir.edu/Courses/ele382/Foo/Tyler_LightSpeed.pdf
9. Nagel HD. Factors influencing patient dose in CT. In: Radiation exposure in computed tomography. Edited by Nagel HD. 2nd ed. Hamberg: Offizin Paul Hartung Druck GmbH & Co; 2000. p. 38-9.
10. Fuchs T, Kachelrieß, Kalender WA. Technical advances in multi-slice spiral CT. Eur J Radiol 2000;36(2):69-73.
11. Rubin GD. Data explosion: the challenge of multidetector-row CT. Eur J Radiol 2000;36(2):74-81.

12. Kalender WA. Computed tomography. New York: John Wiley and Sons; 2000.
13. Brix G, Nagel HD, Stamm G, Veit R, Lechel U, Griebel J, et al. Radiation exposure in multi-slice versus single-slice spiral CT: results of a nationwide survey. Eur Radiol 2003;13:1979-91.
14. Wildberger JE. Dose issue in CT. Available from: URL: http://www.slovakradiology.sk/star/star_2k3/wildberger_dose_issue_ct.pdf
15. Mettler FA, Wiest PW, Locken JA, et al. CT scanning patterns of use and dose. Radiation protection and dosimetry (in press). 2001.
16. Hughes JS. Ionising radiation exposure of the UK population-1999 review. NRPB Report 311. Chilton: NRPB; 1999.
17. McNitt-Gray MF. AAPM/RSNA Physics tutorial for residents: topics in CT. Radiographics 2002;22:1541-53.
18. Olerud HM. CT-dose surveys. Section of dosimetry and medical applications. Norwegian radiation protection authority, P.O. 55 no.1363 Østerås; 178-191.
19. Nagel HD. Fundamentals of CT dosimetry. In: Radiation exposure in computed tomography. Edited by Nagel HD. 2nd ed. Hamberg: Offizin Paul Hartung Druck GmbH & Co; 2000. p. 5-13.
20. European commission. Guidelines on radiation dose to the patient. EUR Report 16262 EN. Brussels: EU; 1999.
21. Shope TB, Gagne RM, Johnson GC. A method for describing the doses delivered by transmission x-ray computed tomography. Med Phys 1981;8(4):488-95.
22. Leitz W, Axelsson B, Szendrö G. Computed tomography dose assessment-a practical approach. Radiat Prot Dosimetry 1995;57(1-4):377-80.
23. Seeram E. Image quality. In: Computed tomography. Edited by Seeram E. 2nd ed. Philadelphia: W.B. Saunders company; 2001. p. 198-218.
24. Reddinger W. CT image quality; 1998. Available from: URL: http://www.t2star.com/modules/CT_IQ.pdf
25. McNitt-Gray MF. Tradeoffs in CT image Quality and dose.
26. European commission. General principles associated with good imaging technique: technical, clinical and physical parameters. Report EUR 16262. Brussels: EU; 1999.
27. Frush DP. Strategies of dose reduction. Pediatr Radiol 2002;32:293-7.

28. Vanderley-Reichner C, Saunders A, Winsor A, McBean K, Dobeli K. Reducing patient dose in CT. The AIR computed tomography advisory panel; 2003. Available from: URL: http://www.a-i-r.com.au/documents.CT_dose_reduce.pdf

29. Hidajat N and Galanski M. Low-dose CT in clinical routine. In: Radiation exposure in computed tomography. Edited by Nagel HD. 2nd ed. Hamberg: Offizin Paul Hartung Druck GmbH & Co; 2000. p. 45.

30. Cohnen M, Fischer H, Hamacher J, Lins E, Kotter R, Modder U. CT of the head by use of reduced current and kilovoltage: relationship between image quality and dose reduction. Am J Neuro Radiol 2000;21:1654-60.

31. Sohaib SA, Peppercorn PD, Horrocks JA, Keene MH, Kenyon GS, Reznek RH. The effect decreasing mAs on image quality and patient dose in sinus CT. Br J Radiol 2001;74(878):157-61.

32. Masashi T, William MM, Manzar A, Arfa K, Zsuzsanna P, Ronald A, et al. Low-dose spiral computed tomography of the thorax: comparison with the standard-dose technique. Invest Radiol 1998;33:68-73.

33. Donnelly LF, Emery KH, Brody AS, et al. Minimizing radiation dose for pediatric body applications of single-detector helical CT: strategies at a large children's hospital. Am J Roentgenol 2001;176:303-6.

34. Crawley MT, Booth A, Wainwright A. A practical approach to the first iteration in the optimization of radiation dose and image quality in CT: estimates of the collective dose saving achieved. Br J Radiol 2001;74(883):607-14.

35. Hamberg LM, Rhea JT, Hunter GJ, Thrall JH. Multi-detector row CT: radiation dose characteristics. Radiology 2003;226(3):762-72.

36. Koller CJ, Eatough JP, Bettridge A. Variation in radiation dose between the same model of multislice CT scanner at different hospitals. Br J Radiol 2003;76(911):798-802.

37. Prasad SR, Wittram C, Shepard J. Mcloud T, Rhea J. Standard-dose and 50% reduce-dose chest CT: comparing the effect on image quality. Am J Roentgenol 2002;179:461-5.

38. Asquier E, Brunereau L, Fauchier F, Bertrand P, Lemarié E and Rouleau P. Multi-slice helical CT scanning of the chest comparison of different "low-dose"

acquisitions. Available from: URL: http://www.toshibaeurope.com/medical/Materials/Visions/Asquier.pdf

39. Macari M, Bini EJ, Xue X, et al. Colorectal neoplasms: prospective comparison of thin-section low-dose multi-detector row CT colonography and conventional colonoscopy for detection. Radiology 2002;224:383-92.
40. Spielmann AL, Heneghan JP, Lee LJ, Yoshizumi T, Nelson RC. Decreasing the radiation dose for renal stone CT: a feasibility study of single- and multidetector CT. Am J Roentgenol 2002;178:1058-62.
41. Kalra MK, Prasad S, Saini S, Blake MA, Varghese J, Halpern EF, et al. Clinical comparison of standard-dose and 50% reduced-dose abdominal CT: effect on image quality. m J Roentgenol 2002;179:1101-6.
42. GE medical systems LightSpeed Plus. Technical reference manual CE 0459. Operator reference: Direction 2281207-100, Rev 2. Copyright©2000, 2001.
43. IMATRON C-150XP/LXP Ultrafast CT scanner. Operator's manual. 1997.
44. PTW-FREIBURG. Instruction manual NOMEX dosemeter.
45. PTW-FREIBURG. User manual ionization chamber type 77336 and type 30009.
46. Edyvean S, Lewis MA, Britten AJ. CT scanner dose survey: measurement protocol version 5.0. ImPACT. 1977.
47. Kelley L. Quality control in computed tomography. In: Quality management in the imaging sciences. Edited by Papp J. 2nd ed. St Louis: Mosby Inc; 2002. p. 198-9.
48. Dorege RT, rin RL. A practical method to measure the MTF of CT scanners. Med Phys 1982;9(5)(Technical notes):758-60.
49. Coltman W. The specification of imaging properties by response to a sine wave input. J Opt Soc Am 1954;44(6):468-71.
50. Droege RT. A practical method to routinely monitor resolution in digital images. Med Phys 1983;10(3)(Technical notes):337-43.
51. Verdun FR, Denys A, Valley JF, Schnyder P, Meuli RA. Detection of low contrast objects: experimental comparison of single-and multi-detector row CT with a phantom. Radiology 2002;223:426-31.
52. Rehani MM, Bongartz G, Kalender W, Golding SJ, Gordon L, Murakami T, et al. Managing patient dose in computed tomography. Version October, 2000: 4.

APPENDIX

APPENDIX

Image quality and radiation dose reproducibility

Before all measurements noise, uniformity and DLP_{air} were checked by following a protocol from the GE LightSpeed Plus technical reference manual.

1.1a Noise and uniformity

1. Take a scan through the water phantom (section 3 of QA phantom) and position a cursor over the resultant image in three different locations.

2. The cursor should be positioned in the center, at the top, and at the side of the image (Figure 1a).

3. At each cursor location, take an ROI measurement and record the standard deviation and mean CT number.

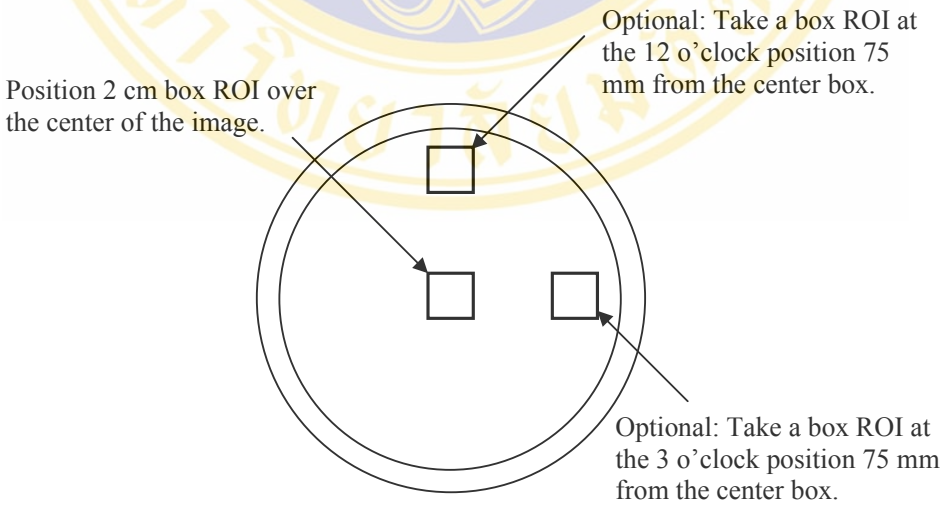

Figure 1a. Test of noise and uniformity (39).

Table 1a. Parameters setting for noise and uniformity tests.

Parameters	Setting
Entry	Head First
Position	Supine
Scan type	Helical HQ mode
Scan range	I0 to S60
Contrast	none
Thickness	10 mm
Table speed	15 mm/sec
Recon interval	10.0 mm
Tile	0 degrees
Scan FOV	Small body
kV	120 kV
mA	190 mA
Rotation speed	1 second
DFOV	25 cm (phantom diameter: approximately 21.5 cm)
Algorithm	Standard and Bone to test high contrast resolution
	Standard to test low contrast detectability
	Standard for pixel value noise and uniformity
Matrix	512
Special process	none

1.2a Radiation dose reproducibility

1. Take 3 exposure readings for the dose in air on axis measurements.
2. Record the DLP_{air} and also measure and record temperature and pressure.

Table 2a. Typical technique for radiation dose reproducibility test.

Parameters	Setting
Scan type	Head-axial
SFOV	25 cm
kV	120 kV
mA	260 mA
Rotation time	1 sec scan
Thickness	5 mm, 4i mode

1.3a Typical results and allowable variations

For noise measurements, the mean of center ROI should equal 0 ± 3 and the standard deviation of the center ROI should equal 3.0 ± 0.4.

For uniformity measurements, the uniformity difference between the center ROI and the average of the edge ROIs should be 0 ± 3.

For dose reproducibility, the variation of the measurements (take 3 exposure reading) should be < 3% variation.

Table 3a. Noise and uniformity.

Exam	slice	Center		12 o'clock		3 o'clock		Average edge mean	uniformity
		mean	SD	mean	SD	mean	SD		
15969	1	-1.41	2.96	-1.74	2.98	-1.77	2.86	-1.76	0.35
	2	-1.66	3.05	-1.98	2.75	-1.98	2.91	-1.98	0.32
15994	1	-1.88	3.07	-2.10	2.96	-1.64	2.94	-1.87	-0.01
	2	-2.06	2.94	-2.18	2.97	-1.94	2.74	-2.06	0.00
16050	1	-1.69	2.98	-2.30	2.97	-1.96	3.09	-2.13	0.44
	2	-1.98	2.85	-2.41	2.82	-2.19	2.85	-2.30	0.32
16667	1	-1.73	2.86	-1.51	2.94	-1.29	2.74	-1.40	-0.33
	2	-1.83	3.00	-1.87	2.74	-1.78	3.10	-1.83	0.00
17156	1	-1.21	2.85	-1.58	2.78	-1.53	2.97	-1.56	0.35
	2	-1.31	2.77	-1.64	2.94	-1.75	2.83	-1.70	0.39
17411	1	-0.89	2.96	-1.28	2.92	-1.26	2.93	-1.27	0.38
	2	-0.88	3.06	-1.49	2.82	-1.50	2.88	-1.50	0.62
19519	1	-0.71	2.76	-1.13	2.91	-0.81	3.08	-0.97	0.26
	2	-0.76	3.04	-1.30	2.90	-0.90	3.11	-1.10	0.34
19685	1	-0.68	2.91	-1.02	2.77	-0.66	3.07	-0.84	0.16
	2	-0.80	2.99	-1.16	2.87	-0.82	2.96	-0.99	0.19
19714	1	-0.82	2.98	-0.92	2.86	-1.54	3.21	-1.23	0.41
	2	-0.91	3.01	-1.18	2.96	-1.67	3.09	-1.43	0.52
19776	1	-0.39	3.10	-0.63	2.90	-0.30	2.77	-0.47	0.08
	2	-0.57	2.80	-0.72	2.78	-0.82	2.88	-0.77	0.20
20660	1	-0.91	2.99	-1.38	2.79	-1.35	3.07	-1.37	0.46
	2	-1.25	2.85	-1.82	2.91	-1.49	2.85	-1.66	0.41

Table 4a. Dose reproducibility.

Date	Offset (nGy/s)	DLP_{air} (mGy.cm)			Average DLP_{air}	T (°C)	mbar P(hPa)	k_D	DPL_{air}	% Diff
		1	2	3						
15/09/03	5.7	10.36	10.36	10.36	10.3600	25.85	1006.5	1.02655	10.635	-
16/09/03	0.0	10.48	10.49	10.49	10.4867	24.95	1007.9	1.02204	10.718	0.78
18/09/03	5.4	10.46	10.46	10.46	10.4600	25.20	1008.9	1.02188	10.689	-0.27
12/10/03	0.0	10.30	10.31	10.31	10.3067	25.90	1004.5	1.02877	10.603	-0.80
4/11/03	0.0	10.49	10.48	10.47	10.4800	22.85	1010.2	1.01253	10.611	0.08
14/11/03	6.0	10.47	10.47	10.48	10.4733	22.80	1011.3	1.01125	10.591	-0.19
30/11/03	0.0	10.71	10.71	10.72	10.7133	22.60	1011.4	1.01047	10.825	2.21*
12/12/03	15.3	10.66	10.66	10.67	10.6633	23.60	1010.5	1.01479	10.821	-0.04
14/12/03	12.6	10.70	10.71	10.71	10.7067	22.70	1012.6	1.00961	10.810	-0.11
23/12/03	3.0	10.67	10.68	10.68	10.6767	24.00	1014.1	1.01255	10.811	0.01
25/12/03	16.2	10.59	10.59	10.59	10.5900	24.40	1009.9	1.01813	10.782	-0.27
27/12/03	18.6	10.58	10.58	10.59	10.5833	24.85	1012.4	1.01716	10.765	-0.16
29/12/03	0.0	10.73	10.73	10.73	10.7300	22.30	1014.1	1.00676	10.802	0.35
30/12/03	3.9	10.68	10.68	10.69	10.6833	22.80	1014.9	1.00767	10.765	-0.34
9/01/04	0.0	10.58	10.60	10.59	10.5900	22.50	1013.6	1.00794	10.674	-0.85
17/01/04	4.2	10.65	10.67	10.67	10.6633	22.90	1014.5	1.00840	10.753	0.74
22/01/04	13.8	10.60	10.60	10.60	10.6000	22.50	1009.7	1.01183	10.725	-0.26
24/01/04	0.0	10.67	10.68	10.67	10.6733	22.30	1010.6	1.01024	10.783	0.53
5/02/04	26.4	10.53	10.54	10.53	10.5333	23.20	1007.0	1.01694	10.712	-0.66
6/02/04	14.4	10.49	10.50	10.50	10.4967	25.80	1010.7	1.02212	10.729	0.16
11/02/04	12.9	10.57	10.58	10.58	10.5767	22.70	1013.9	1.00832	10.665	-0.60
12/02/04	11.7	10.57	10.57	10.56	10.5667	22.50	1013.9	1.00764	10.647	-0.16
14/02/04	5.4	10.56	10.57	10.56	10.5633	23.70	1013.7	1.01193	10.689	0.39
19/03/04	7.8	10.41	10.42	10.42	10.4167	24.60	1007.5	1.02124	10.638	-0.48

* New x-ray tube replacement (19 November 2003)

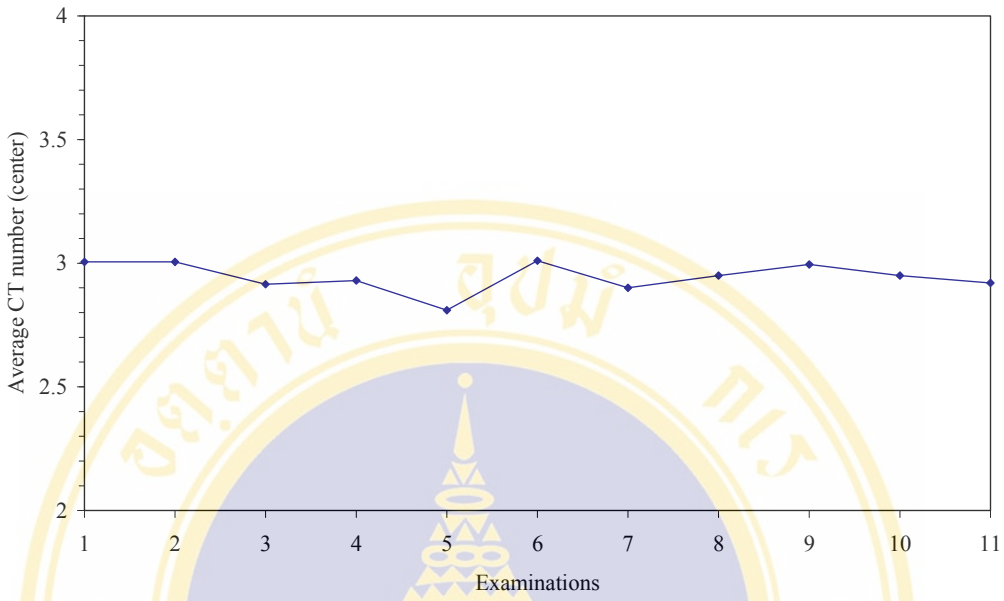

Figure 2a. CT number (HU) variation of the multi-detector CT, average with two slices, throughout the period of this experimental study.

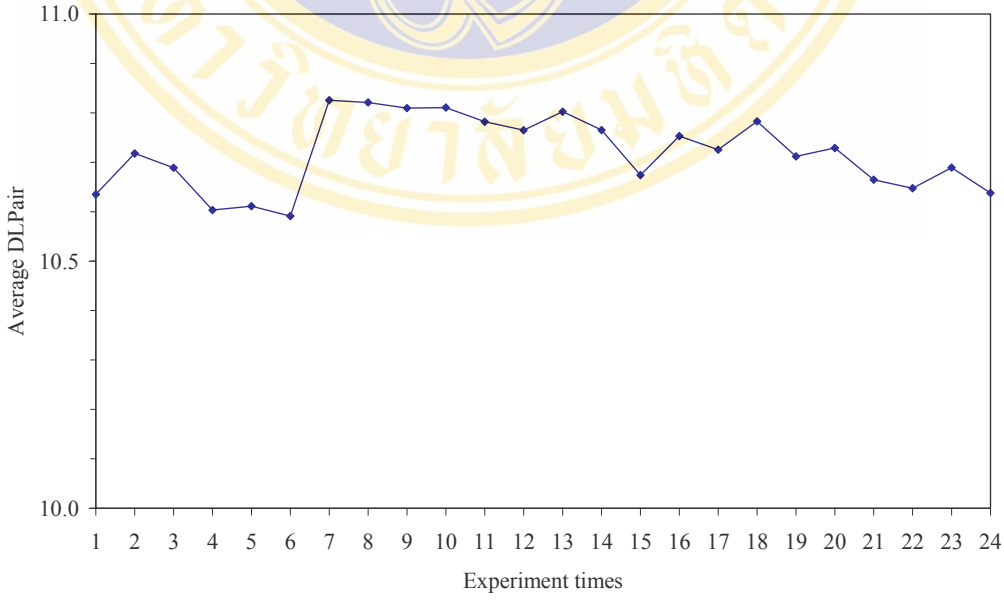

Figure 3a. Dose variation (DLP_{air}) of the multi-detector CT throughout the period of this experimental study**.**

BIOGRAPHY

NAME Miss Pimolpun Changkaew

DATE OF BIRTH 5 April 1979

PLACE OF BIRTH Chiyaphum, Thailand

INSTITUTIONS ATTENDED Mahidol University, 2001:
Bachelor of Science
(Radiological Technology)

Mahidol University, 2005:
Master of Science
(Medical Physics)

HOME ADDRESS 232 Moo 5, Tambon Ban-kor, Amphua Muang, Nakhonrajsima, 30000
Tel. 044-296331
E-mail: kangkokkururu@yahoo.com